Doctoral thesis

Induced charge density wave and superconductivity in Cu-doped $TaSe_3$

Atsushi Nomura

Department of Applied Physics,
Hokkaido University

March 2019

Abstract

The relationship between superconductivity (SC) and charge density wave (CDW) has been a major research topic in condensed matter physics and has been investigated in many materials. However, previous studies were actually limited to two cases: the first is where SC and a CDW intrinsically exist; the second is where SC is induced in a CDW material. To understand the whole picture of the relationship between SC and CDW, we investigated the relationship in a third case where a CDW is induced in a superconducting material.

Transition metal trichalcogenides, MX_3 (M: Nb, Ta; X: S, Se), has a structure consisting of chains made of transition metals and chalcogens, and the chains are weakly bonded by van der Waals forces. Owing to this structure, MX_3 is a quasi-one-dimensional conductor in which an electric current travels well in the direction of the chain axis. In most materials belonging to MX_3 ($NbSe_3$, TaS_3, and NbS_3), the Fermi surface is close to a plane. Therefore, the nesting condition is good and a CDW develops below the transition temperature in these materials. On the other hand, $TaSe_3$ which is one of MX_3 exhibits no CDW transition but the filamentary superconductivity transition at about 2 K because $TaSe_3$ is more three-dimensional than the other MX_3 compounds.

If Cu atoms are doped in $TaSe_3$, the Cu atoms are considered to be difficult to substitute for Ta atoms because the common valence that Cu takes (+1 or +2) is different from that of Ta (+5). On the other hand, the Cu atoms are expected to enter in the Van der Waals gap and to increase the distance between chains of $TaSe_3$. Therefore, it is presumed that Cu doping decreases the dimensionality and improves the nesting condition in $TaSe_3$.

In this thesis, we tried to induce a CDW in $TaSe_3$ with a superconducting material by Cu doping, and investigated the relationship between the induced CDW and SC.

We have synthesized single crystals of Cu-doped $TaSe_3$, and measured precisely the temperature dependence of the resistance from 4.2 to 280 K. We discover an anomalous sharp dip in the temperature derivative of the resistance (dR/dT) at about 91 K in Cu-doped $TaSe_3$, which is never observed in pure $TaSe_3$. The dip suggests that there is a

sudden change in state with a relative increase in resistance. In addition, the dip is "γ" shaped. We reveal that the same "γ"-shaped dip in $\mathrm{d}R/\mathrm{d}T$ is commonly observed at the CDW transition temperature in many CDW conductors, which is a universal consequence resulting from the opening and growth of a CDW gap on a Fermi surface. Furthermore, the result of the single-crystal X-ray diffraction (XRD) analysis implies that the lattice parameters perpendicular the chain axis increase and that parallel to the chain axis decreases by Cu doping, leading to an improvement in the nesting condition. The "γ"-shaped dip and the result of the single-crystal XRD analysis show that a CDW emerges by Cu doping in $TaSe_3$.

We investigated the effect of Cu doping on SC in Cu-doped $TaSe_3$ by measuring the temperature dependence of the resistance from 0.6 to 2 K. We observed an emergence of a region where the SC transition temperature (T_C) decreased in samples with higher Cu concentrations, and found that the region tended to expand with increasing Cu concentration. These results and the fact that the SC of $TaSe_3$ is filamentary show that SC is suppressed locally by Cu doping in Cu-doped $TaSe_3$.

From the above discussions, it was revealed that a CDW is induced while SC is suppressed in Cu-doped $TaSe_3$. Hence, the induced CDW and SC would be in a competitive relationship.

The locality of SC suppression suggests that the induced CDWs are local. The resistance anomaly due to the induced CDW transition was extremely small. Moreover, the size of the anomaly was enhanced with increasing Cu concentration but the temperature at which the anomaly appeared hardly changed. These results of the anomaly can be interpreted consistently from the short-range order of the induced CDWs in the vicinity of Cu atoms.

From all the discussions, we conclude that the induced short-range order CDWs and SC are in a competitive relationship in Cu-doped $TaSe_3$. The competitive relationship between short-range order CDWs and SC obtained in the present work is different from the non-competitive relationship previously reported in Cu_xTiSe_2 where SC is induced in a CDW material. By comparing the detailed experimental results of these two materials, we will clarify the physics that defines the relationship between short-range order CDWs and SC.

Contents

Outline of this thesis

This thesis is organised as follows. In chapter 1, we explain the significance of the induction of a charge density wave (CDW), the unresolved question about the relationship between CDW and superconductivity (SC), and the purpose of this study. In chapter 2, we explain $TaSe_3$ of a superconducting material and Cu doping which is a method capable of inducing a CDW in $TaSe_3$. We report experiment results from 4 K to 280 K in Cu-doped $TaSe_3$ and discuss the presence of a CDW. In chapter 3, we report the results of the resistance mesurement from 0.6 K to 4.2 K in Cu-doped $TaSe_3$ and discuss the effect of Cu doping on SC. In chapter 4, we discuss the relationship between the induced CDW and SC, and the short-range order of the induced CDWs in Cu-doped $TaSe_3$. Moreover, we compare the relationship between the short-range order CDWs and SC in Cu-doped $TaSe_3$ with that in another material and suggest a new parameter that influences the relationship between short-range order CDWs and SC.

Chapter 1

General introduction

1.1 Induction of macroscopic quantum state

The induction of superconductivity (SC) has helped in the search for new superconducting characteristics and in answering unresolved questions about SC. For example, high-temperature SC has been induced by doping carriers in insulators [1]. As a result, a new SC mechanism was found, and the transition temperature (T_C) achieved 164 K under high pressure [2]. In addition, it was found that conventional SC appears in a sulfur hydride system under high pressure [3]. This discovery brought the leap of T_C to 203 K and showed the possibility of realizing a higher T_C in other hydrogen-based materials. Moreover, SC was induced in some charge density wave (CDW) compounds by employing doping or high pressure, and the coexistence or competition of induced SC with CDW was investigated [4, 5, 6, 7, 8, 9]. Thus, the induction of SC provides many opportunities to study SC.

CDW is a macroscopic quantum state as well as SC. CDWs occur in low-dimensional metals as the result of the Peierls instability of Fermi surface. Previous CDW studies have provided a lot of knowledge about the mechanisms and the dynamics of CDW by targeting materials with intrinsic CDW states [10, 11]. However, the next stage of this research should involve inducing a CDW in materials that do not normally exhibit a one, because new CDW characteristics might be obtained and it will provide many opportunities to deal with unresolved issues as well as SC. For example, new driving mechanisms other

than conventional Fermi surface nesting might be found as reported for $NbSe_2$ [12] and $TiSe_2$ [13]. Moreover, if a CDW is induced in materials that exhibit SC, we can study the relationship between induced CDW and SC.

1.2 Relationship between charge density wave (CDW) and superconductivity

The relationship between CDW and SC has been a major research topic in condensed matter physics. For example, in $ZrTe_3$ in which a CDW and SC exist under atmospheric pressure, the application of pressure below 2 GPa enhances the CDW and eliminates the SC transition as shown in Fig. 1.1 [14]. On the other hand, the CDW is suppressed above 2 GPa while the SC transition emerges again at $\sim$5 GPa. Moreover, in $NbSe_3$ with a typical CDW material, Ta doping suppresses two CDWs and induces the SC transitionas as shown in Fig. 1.2 [15]. These results show that the CDW or the SC is enhanced while the other is suppressed, which is ascribed to the competition between the CDW and SC on a Fermi surface. On the other hand, in a Cu_xTiSe_2 system where Cu atoms are doped in $1T$-$TiSe_2$ with a commensurate CDW material, a unique CDW and SC phase diagram is observed as shown in Fig. 1.3 and a new relationship between CDW and SC has been discussed [5, 16, 17]. According to the temperature dependence of the resistance, the CDW is suppressed by Cu doping while SC is induced, and the dependence of the SC transition temperature (T_C) on Cu concentration has a domelike structure [5]. However, precise measurements performed with scanning tunneling microscopy (STM) and X-ray diffraction (XRD) reveal that short-range order CDWs survive up to high Cu concentrations where the SC emerges and the transition temperature of the short-range order CDWs is independent of the T_C [16, 17]. This result suggests that short-range order CDWs are not necessarily in competition with SC and cannot be explained solely in terms of the competition for the density of states at the Fermi level. Moreover, according to the XRD result, the short-range order CDWs change from commensurate to incommensurate at the Cu concentration where SC emerges in Cu_xTiSe_2 [17]. The result suggests that the incommensuration of the CDWs may affect the relationship between the CDWs and SC. However, the reason for this is unclear. As described above, the relationship between CDW and SC has been investigated in many materials. However, previous studies were

actually limited to two cases as shown in Table 2.2: the first is where a CDW and SC intrinsically exist; the second is where SC is induced in a CDW material. Here, in addition to these two cases, we should also investigate the relationship in a third case where a CDW is induced in a superconducting material, if we are to understand the whole picture of the relationship.

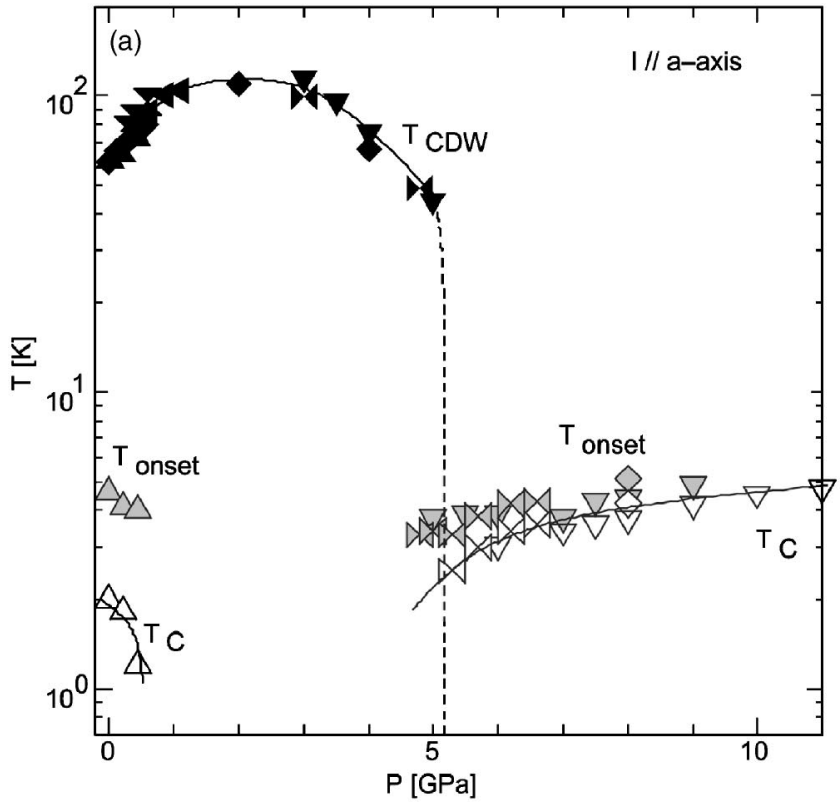

Figure 1.1: Pressure dependence of the CDW transition temperature T_{CDW} , the superconducting transition temperature T_{C} and the onset temperature of superconducting transition T_{onset} for $ZrTe_3$ [14].

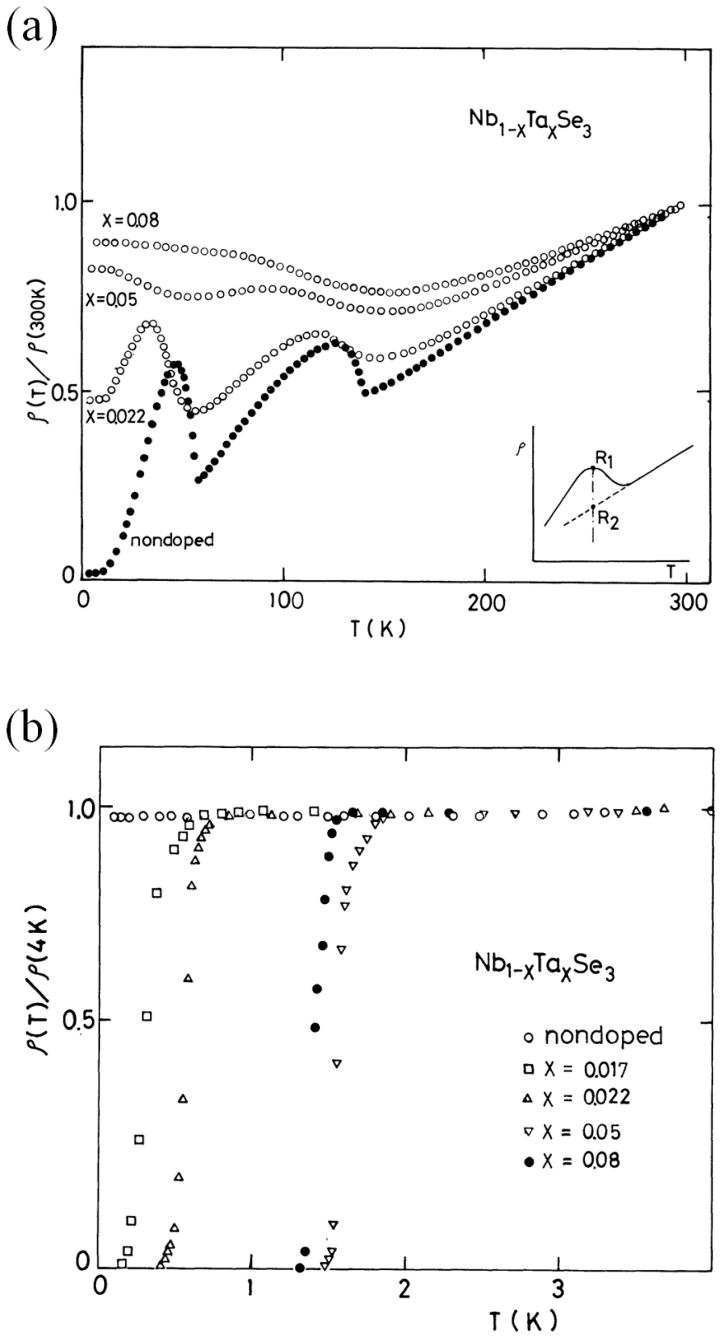

Figure 1.2: The temperature dependence of the resistivity of the non-doped and doped $NbSe_3$ [15]. (a)High temperature range. The resistivity is normalized to the value at 300 K. (b)Low temperature range. The resistivity is normalized to the value at 4 K.

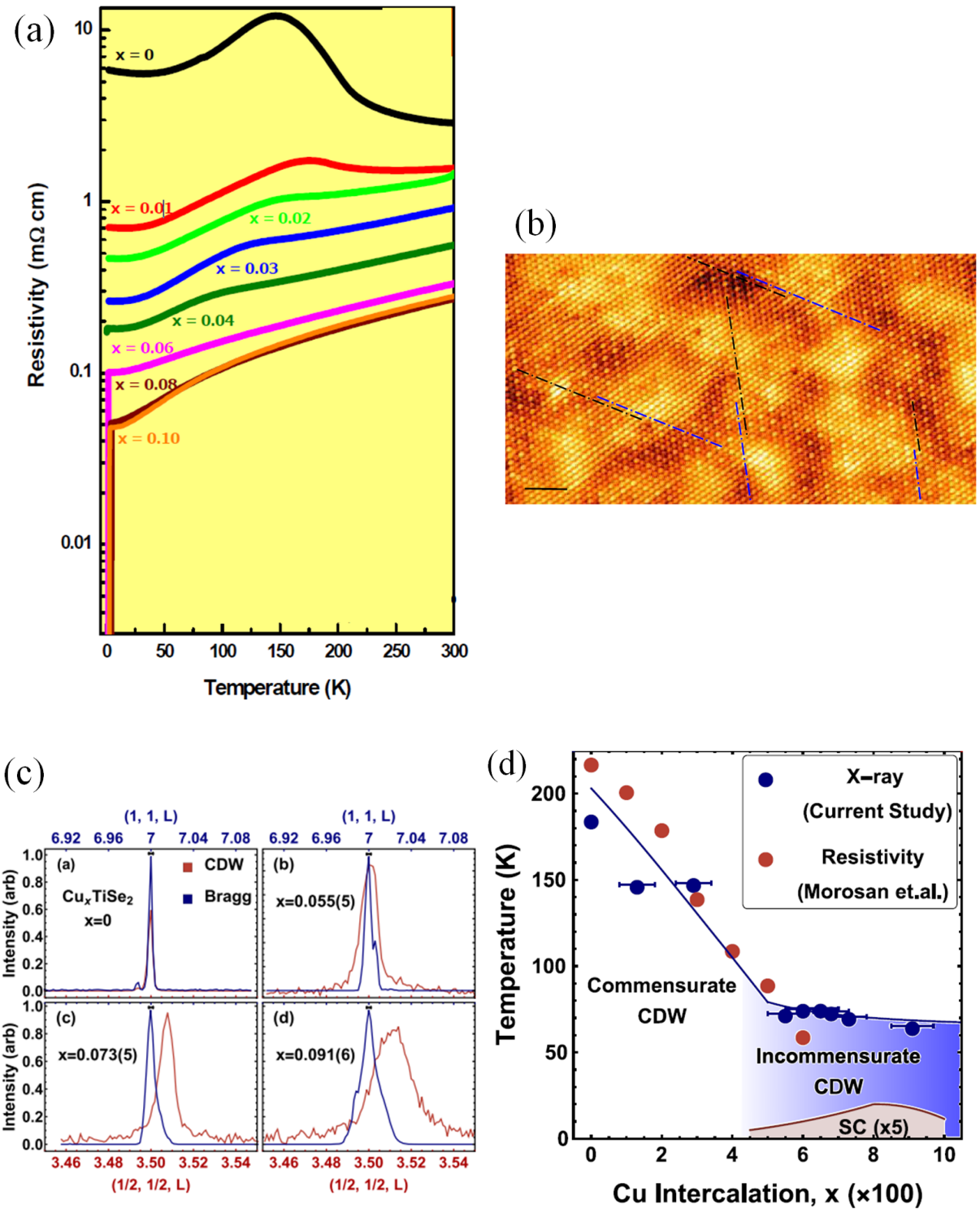

Figure 1.3: (a)The temperature dependence of the resistivity of Cu_xTiSe_2 [5]. (b)STM micrograph (V_{bias}=10 mV, I_t=60 pA) of $Cu_{0.07}TiSe_2$ at 1.2 K [16]. The dashed blue and black lines highlight the π-phase shift between neighbouring CDW domains. Scale bar=2 nm. (c)Simultaneous L cuts of the (1,1,7) Bragg peak as well as the (1/2,1/2,7/2) CDW superlattice peak for various amounts of Cu concentration in Cu_xTiSe_2 [17]. Data for x=0, 0.055, 0.073, and 0.091 were taken at 50 K, 11 K, 15 K, and 20 K, respectively. Momentum resolution is indicated with the black line above the peaks. (d)The phase diagram for Cu_xTiSe_2 [17]. The blue points were obtained in Ref. [17]. The red points and the line delineating the superconducting region are from Ref. [5].

Table 1.1: The relationship between SC and CDW.

①SC and CDW intrinsically exist in a material (e.g.: $ZrTe_3$ under pressure [14])	Competition
②SC is induced in a CDW material (e.g.: Ta_xNbSe_3 [15], Cu_xTiSe_3 [5, 16, 17])	Competition (Long-range order CDW) Non-competition (Short-range order CDW)
③CDW is induced in a SC material	???

1.3 Purpose of this study

In this thesis, we induced a CDW in a superconducting material and investigated the relationship between the induced CDW and SC.

Chapter 2

Emergence of a CDW in Cu-doped $TaSe_3$

2.1 Introduction

2.1.1 $TaSe_3$

$TaSe_3$ is a predominant candidate superconducting material capable of inducing a CDW. $TaSe_3$ is one of the transition metal trichalcogenides, MX_3 (M: Nb, Ta; X: S, Se). MX_3 has a structure consisting of chains made of transition metals and chalcogens, and the chains are weakly bonded by van der Waals forces [18, 19, 20, 21]. Figure 2.1 shows the structure of $TaSe_3$ [22]. Owing to this structure, MX_3 is a quasi-one-dimensional conductor in which an electric current travels well in the direction of the chain axis (b-axis). In most materials belonging to MX_3 ($NbSe_3$, TaS_3, and NbS_3), the Fermi surface of is close to a plane [23]. If the Fermi surface was translated by a wave vector, it would overlap well with that before translation, i.e., the nesting condition is good. This indicates the intrinsic instability of the Fermi surface, and as a result, a CDW develops below the transition temperature as shown in Fig. 2.2 [24, 25, 26]. On the other hand, $TaSe_3$ exhibits different properties from the other MX_3. $TaSe_3$ is more three-dimensional than the other MX_3 compounds. Actually, the electrical conductivity anisotropy ($\sigma_{\parallel} / \sigma_{\perp}$) of $TaSe_3$ is 3–15, while that of TaS_3 is $\sim$100 and that of $NbSe_3$ is 10–20 [28, 29, 30, 31]. Furthermore, according to the band calculation, $TaSe_3$ has two-dimensional Fermi surfaces, which are described as fused tunnels running in the $(-a^* + c^*)$ direction in contrast to the one-dimensional flat

Fermi surfaces of $NbSe_3$ and TaS_3 [23]. Therefore, $TaSe_3$ exhibits no CDW transition over the entire temperature range, but the superconductivity transition occurs at about 2 K [22, 32, 33].

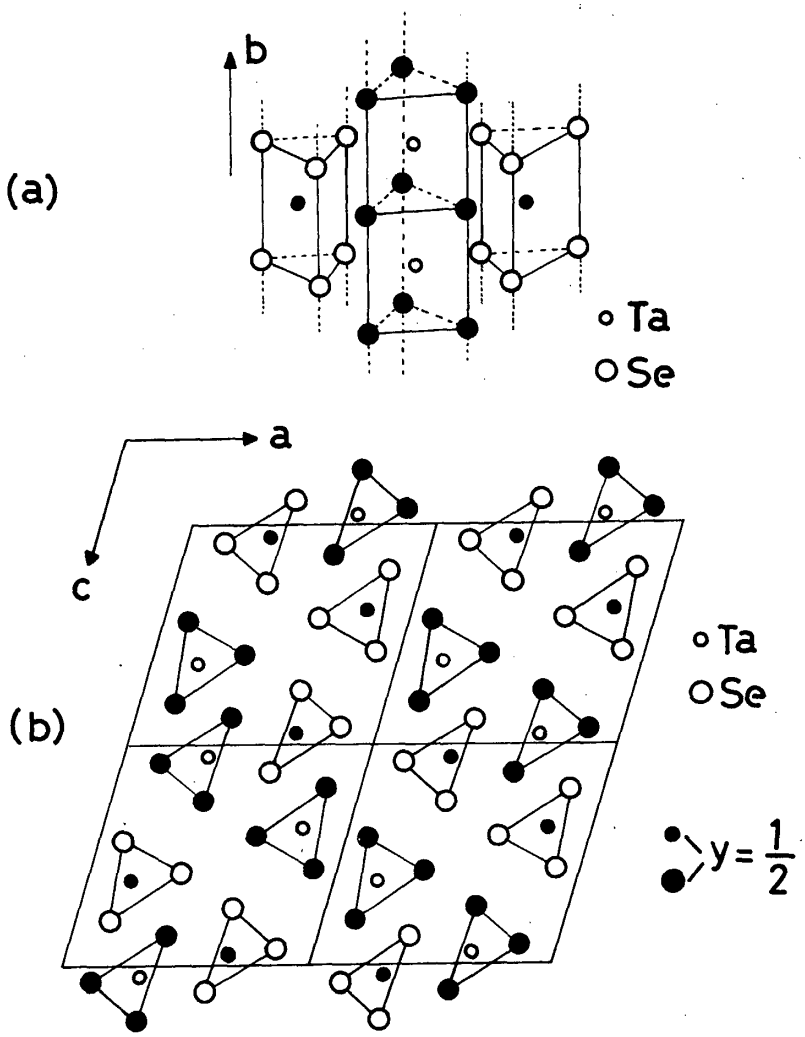

Figure 2.1: Structure of TaS_3 [22]. (a) Stacking along the *b*-axis. (b) Projection of the structure on the (010) plane.

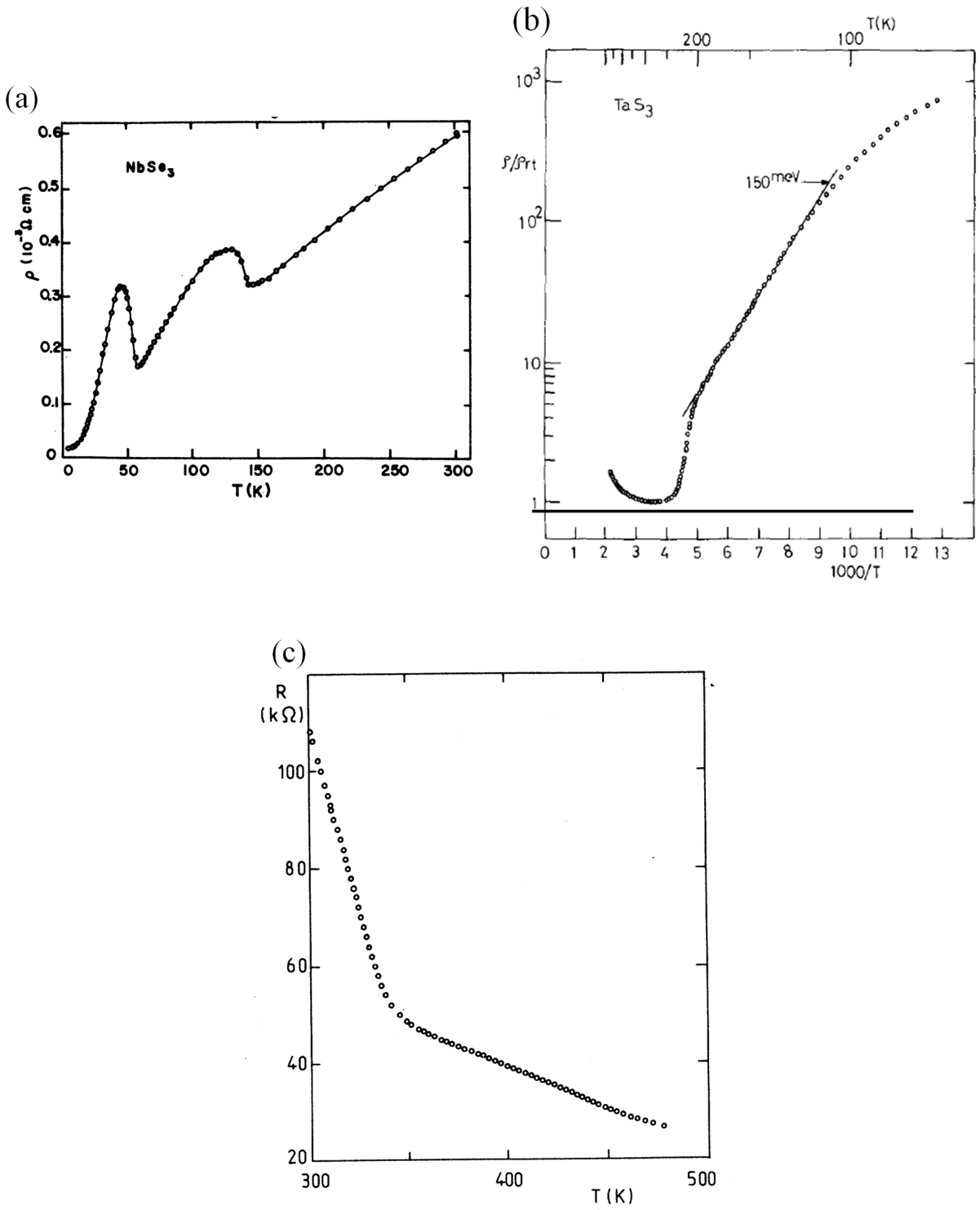

Figure 2.2: (a)The temperature dependence of the resistivity of NbS_3 [24]. (b)The temperature dependence of the resistivity of TaS_3 [25]. (c)The temperature dependence of the resistivity of NbS_3 [26].

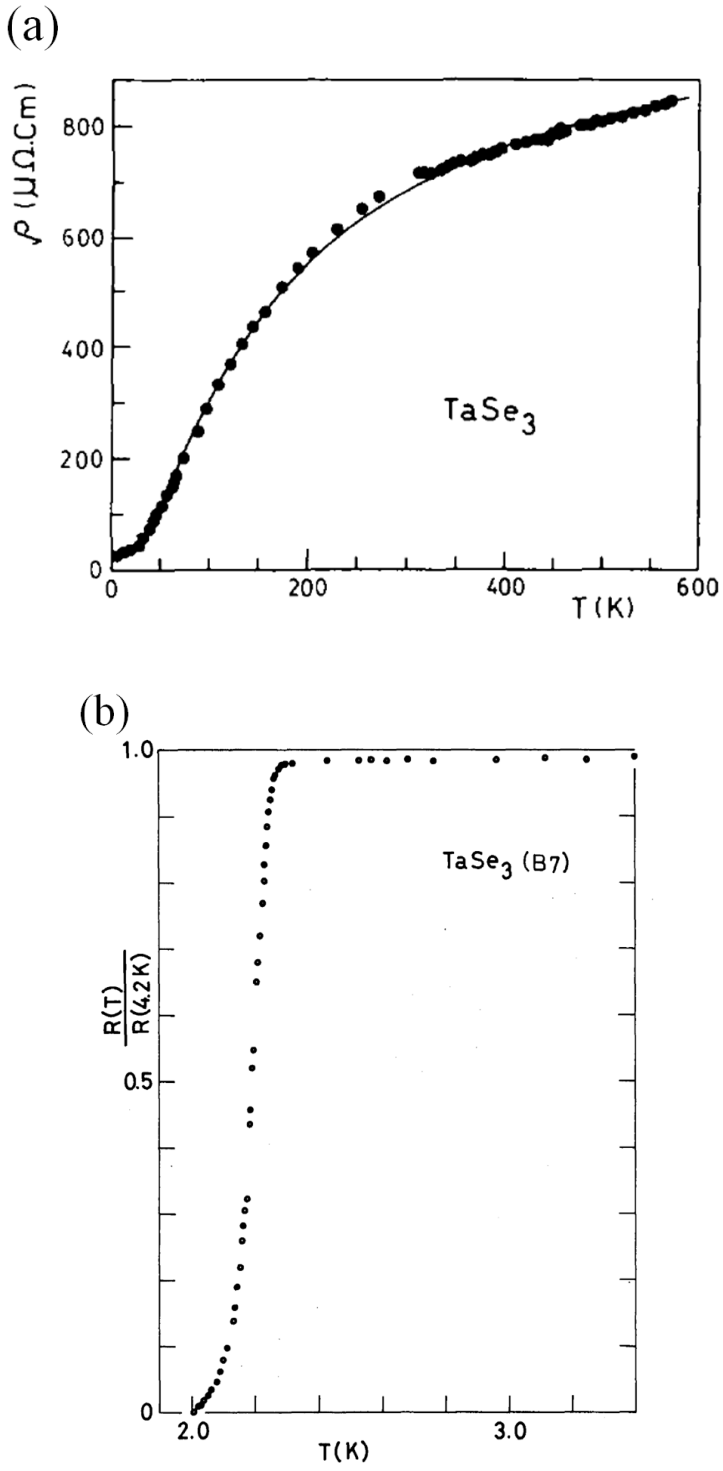

Figure 2.3: The temperature dependence of the resistivity of $TaSe_3$. (a)High temperature range [32]. (b)Low temperature range [22].

2.1.2 Cu doping

There is Cu doping as a predominant candidate method capable of inducing a CDW in $TaSe_3$. If Cu atoms are doped in $TaSe_3$, the Cu atoms are considered to be difficult to substitute for Ta atoms because the common valence that Cu takes (+1 or +2) is different from that of Ta (+5). On the other hand, because the $TaSe_3$ chains are weakly bonded by Van der Waals forces, the Cu atoms are expected to enter in the Van der Waals gap and to increase the distance between chains. Actually, in Cu_xTiSe_2 where $TiSe_2$ layers are weakly bonded by Van der Waals forces, Cu atoms enter between layers and increase the distance between layers [5, 16]. Therefore, it is presumed that Cu doping for $TaSe_3$ decreases the overlap between electron wave functions perpendicular to the chain axis, leading to a decrease in dimensionality. As a result, the nesting condition may be improved.

2.1.3 Purpose of this study

In this chapter, we tried to induce a CDW in $TaSe_3$ with a superconducting material by Cu doping, and investigated the presence of a CDW by measuring the resistance as a function of temperature.

2.2 Experimental

2.2.1 Synthesis of single crystals

We prepared single crystals of pure $TaSe_3$ and Cu-doped $TaSe_3$ synthesized by the vapor phase transport method. We obtained three kinds of Cu-doped $TaSe_3$ crystals by changing the nominal value of Cu (x) and the growth temperature as shown in Table. 2.1. First, we prepared Ta, Se and Cu materials (99.95%, 99.999%, and 99.9% respectively, Nilaco Corp.) with a molar ratio of 1 to 3 to x, which are one gram in total. These materials were sealed in an evacuated 10.5-mm-diam 20-cm-long quartz tube. The tube was then heated at 678°C or 708°C, and maintained at the temperature for about seven days. Finally, the tube was quenched in water. In this way, we obtained single crystals as shown in Fig. 2.4. The crystals are ribbon-shaped with a typical dimensions of $5\,\mu\mathrm{m} \times 10\,\mu\mathrm{m} \times 5\,\mathrm{mm}$. The ribbon plane is $(\bar{2}01)$ [22].

Table 2.1: The synthesis condition of pure $TaSe_3$ and Cu-doped $TaSe_3$.

Crystal	Nominal value of Cu (x)	Growth temperature
pure $TaSe_3$	0	678°C
Cu-doped $TaSe_3$ A	0.0075	678°C
Cu-doped $TaSe_3$ B	0.05	678°C
Cu-doped $TaSe_3$ C	0.05	708°C

Figure 2.4: Single crystals of Cu-doped $TaSe_3$ in a quartz tube.

2.2.2 Inductively coupled plasma atomic emission spectroscopy

To examine the actual concentration of Cu in the crystals, we performed inductively coupled plasma atomic emission spectroscopy (ICP-AES) using an ICPE-9000 (Shimadzu Corp.). We determined the average Cu concentration for a bundle of the whisker crystals (a few milligrams).

2.2.3 Single-crystal X-ray diffraction (XRD)

The crystal structure was examined by single-crystal X-ray diffraction (XRD) analysis with Cu Kα radiation ($\lambda = 1.5418\,\text{Å}$) using a Rigaku XtaLAB P200 diffractometer. The lattice parameters were extracted by fitting the XRD spectra using CrysAlisPro.

2.2.4 Resistance measurement

The temperature dependence of the resistance along the b-axis (parallel to the chain axis) was precisely measured with a dc four-probe measurement. The whisker crystal was cut to about 2 mm. Current terminals were attached to both ends of the crystal with carbon paste, and voltage terminals were attached inside as shown in Fig. 2.5. The cross-section at both ends of the crystal was covered with carbon paste. We measured the temperature dependence of the resistance while the samples were warmed from 4.2 to 280 K for about 30 hours. The temperature was measured with a Cernox resistance sensor.

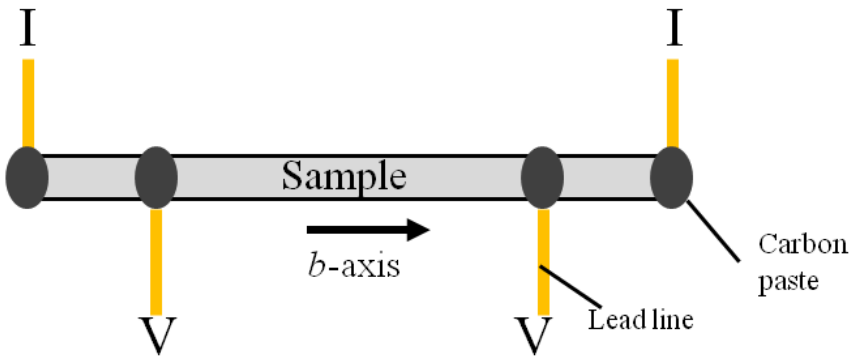

Figure 2.5: Schematic of the arrengement of the current terminals and the voltage terminals.

2.3 Results

2.3.1 Crystal

The result of ICP-AES are listed in Table 2.2. From the ratio of the amount of substance determined by ICP-AES, we define the Cu concentration as the ratio of Cu to Ta given as a percentage. The Cu concentrations of the Cu-doped $TaSe_3$ were $0.51 \pm 0.10\%$, $0.95 \pm 0.10\%$ and $1.12 \pm 0.10\%$. Thus, together with pure $TaSe_3$, we prepared four kinds of crystals with different Cu concentrations. The Cu concentration did not exceed 1.2% even when the nominal value for Cu was more than 5%.

Table 2.2: The result of ICP-AES.

Crystal	Nominal value of Cu (x)	Growth temperature	Ratio of amount of substance		
			Ta	Se	Cu
pure $TaSe_3$	0	678°C	1	2.79 ± 0.10	0
Cu-doped $TaSe_3$ A	0.0075	678°C	1	2.86 ± 0.10	0.0051 ± 0.0010
Cu-doped $TaSe_3$ B	0.05	678°C	1	2.91 ± 0.10	0.0095 ± 0.0010
Cu-doped $TaSe_3$ C	0.05	708°C	1	2.89 ± 0.10	0.0112 ± 0.0010

2.3.2 Result of single-crystal XRD

Figure 2.6 shows the lattice parameters determined by single-crystal XRD analysis as a function of Cu concentration. The crystal structure of $TaSe_3$ is monoclinic. The a-axis and c-axis are perpendicular to the b-axis, which is the direction of the chain axis, and β is the angle between the a-axis and the c-axis. The lattice parameters obtained for three samples of pure $TaSe_3$ were $a = 10.402-10.409\,\text{Å}$, $b = 3.498-3.500\,\text{Å}$, $c = 9.824-9.828\,\text{Å}$ and $\beta = 106.24-106.27°$, which showed little sample dependence. However, the obtained values were in good agreement with previously reported values of $a = 10.402 \pm 0.004\,\text{Å}$, $b = 3.495 \pm 0.002\,\text{Å}$, $c = 9.829 \pm 0.004\,\text{Å}$, $\beta = 106.26 \pm 0.03°$ [19], and $a = 10.374\,\text{Å}$, $b = 3.501\,\text{Å}$, $c = 9.827\,\text{Å}$, $\beta = 106.11°$ [34]. The lattice parameters we obtained for three samples of each Cu-doped $TaSe_3$ also exhibited sample dependence in almost the same range as that of pure $TaSe_3$. The Cu concentration dependence of lattice parameters doesn't show a clear change which satisfies Vegard's law. However, the average values for the a-axis, c-axis and β tended to increase slightly as the Cu concentration increased, while that of the b-axis tended to decrease slightly.

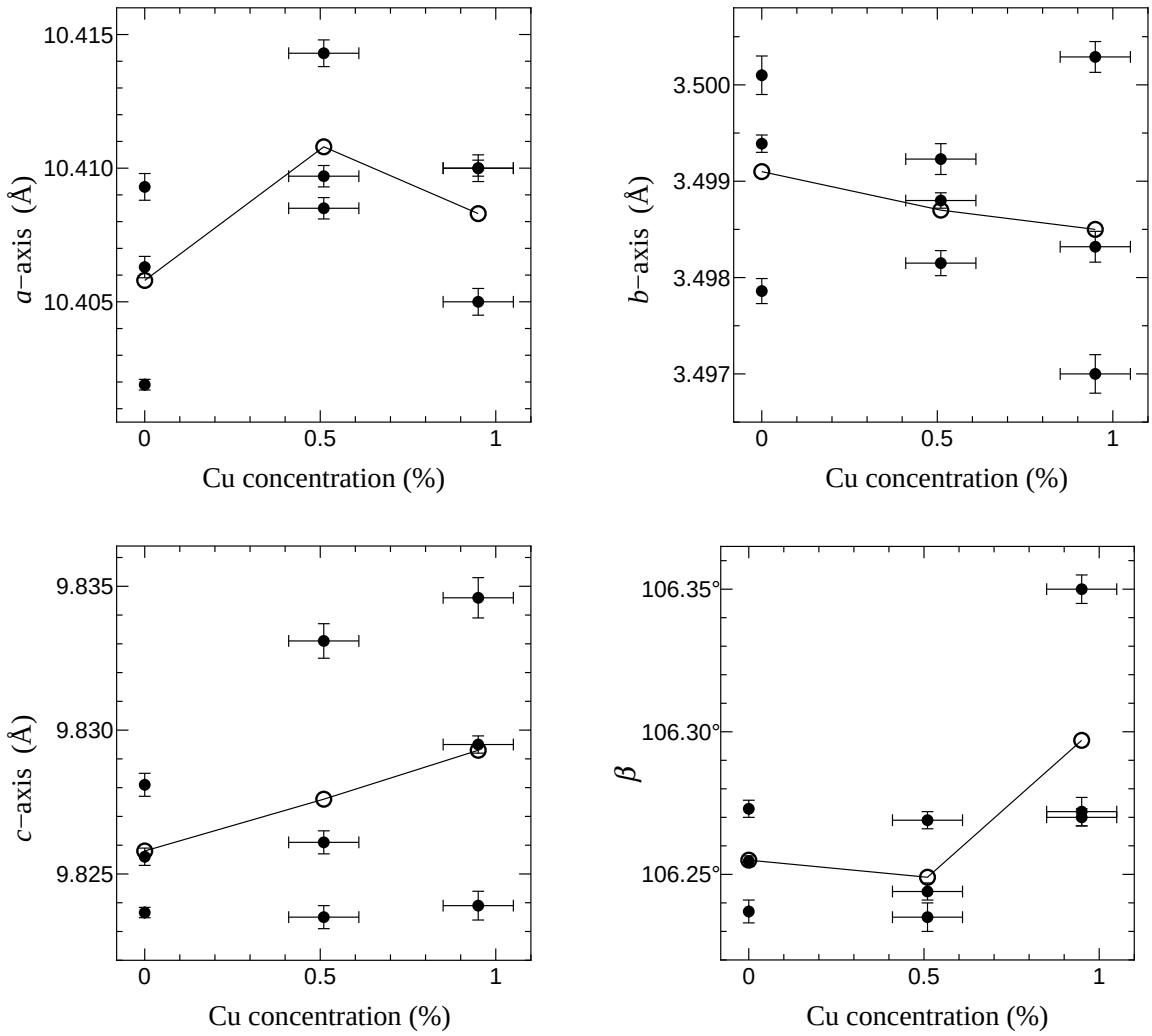

Figure 2.6: The lattice parameters of pure $TaSe_3$ and Cu-doped $TaSe_3$ determined by single-crystal XRD analysis. Three samples for each Cu concentration are measured. The filled circles show the data for each sample, and the open circles show the average value for each Cu concentration.

2.3.3 Resistance measurement results from 4.2 K to 280 K

The temperature dependence of the resistance was measured for several samples for each Cu concentration. Figure 2.7 shows typical data for pure $TaSe_3$ and Cu-doped $TaSe_3$. In all the samples, as the temperature increased, the resistance monotonically increased with a convex downward curvature in the low temperature range ($T < 70\,\mathrm{K}$) and with a convex upward curvature in the high temperature range ($T > 70\,\mathrm{K}$) unlike the linear R-T curve for typical metals. The residual resistance ratios ($RRR = R(280\,\mathrm{K}) \,/\, R(4.5\,\mathrm{K})$) were 43.2–57.1 in pure $TaSe_3$, 5.3–6.3 in Cu-doped $TaSe_3$ (0.51%), 3.2–3.5 in Cu-doped $TaSe_3$ (0.95%) and 3.0–3.3 in Cu-doped $TaSe_3$ (1.12%). The RRR decreased with increasing Cu concentration.

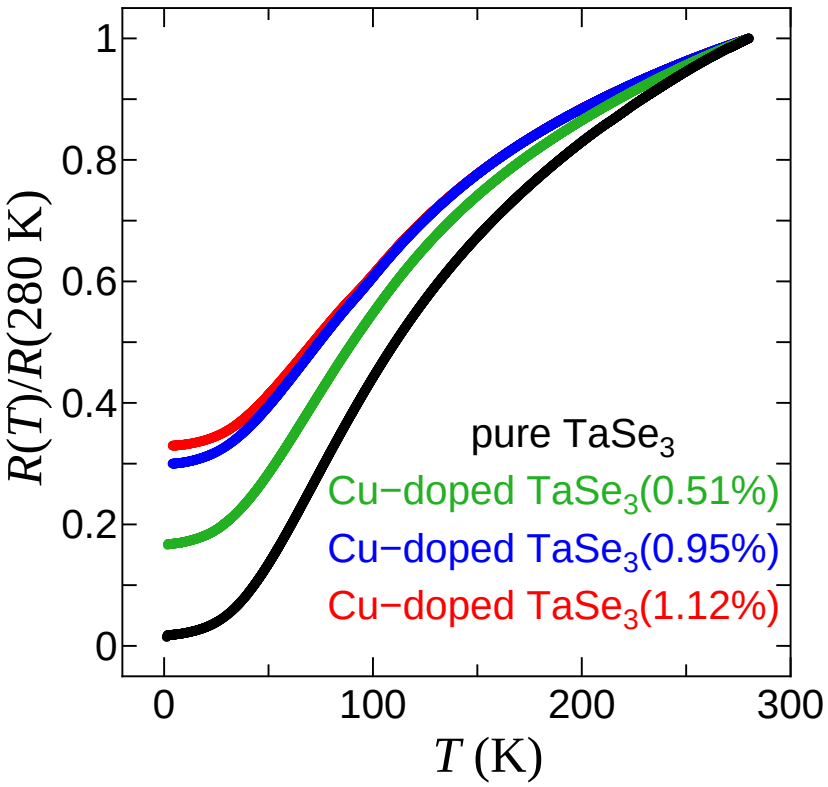

Figure 2.7: The temperature dependence of the resistance normalized by the resistance at 280 K of pure $TaSe_3$ and Cu-doped $TaSe_3$.

Figure 2.8(a) shows the temperature dependence of the resistance normalized by the difference between the resistance at 4.5 K and that at 280 K to compare the temperature dependent parts of the resistance of pure $TaSe_3$ and Cu-doped $TaSe_3$. The temperature dependence of the resistance shows almost the same functional form for all samples. As the Cu concentration increased, the normalized resistance at 4.5 K increased almost as a linear function of the Cu concentration as shown in Figure 2.8(b). Therefore, Matthiessen's rule holds for the Cu-doped $TaSe_3$ system.

To compare these temperature dependences of the resistance in detail, we plot the temperature derivative of the resistance ($\mathrm{d}R/\mathrm{d}T$) in Fig. 2.8(c). In pure $TaSe_3$, the $\mathrm{d}R/\mathrm{d}T$ increased monotonically from 4.5 K, showed a maximum of 70 K, and decreased monotonically above 70 K. In all Cu-doped $TaSe_3$ with different Cu concentrations, the $\mathrm{d}R/\mathrm{d}T$ showed a similar temperature dependence to that of pure $TaSe_3$ over almost the entire temperature range. However, there was an anomalous sharp dip in the $\mathrm{d}R/\mathrm{d}T$ at about 91 K in Cu-doped $TaSe_3$, but never in pure $TaSe_3$. In Cu-doped $TaSe_3$ (1.12%) with the maximum Cu concentration, the $\mathrm{d}R/\mathrm{d}T$ suddenly decreased from about 102 K to about 91 K, showed a narrow minimum, and began to increase at about 91 K. Below about 91 K, it gradually returned to a temperature dependence similar to that of pure $TaSe_3$. In summary, the anomalous sharp dip was "γ" shaped. The depth of the dip increased with increasing Cu concentration. We call the temperature at which the $\mathrm{d}R/\mathrm{d}T$ drops most the dip appearance temperature, T_{dip}. The T_{dip} was observed as 92 ± 2 K and 91 ± 2 K for Cu concentrations of 0.95% and 1.12%, respectively. There was no significant difference between the T_{dip} values of Cu-doped $TaSe_3$ (0.95%) and Cu-doped $TaSe_3$ (1.12%) beyond the measurement accuracy (± 2 K). In Cu-doped $TaSe_3$ (0.51%), the dip was too small to define the minimum $\mathrm{d}R/\mathrm{d}T$. The dip was reproduced in all samples measured for the same Cu concentration. Furthermore, the same T_{dip} was observed by cooling and heating the Cu-doped $TaSe_3$ (1.12%) sample, that is, no thermal hysteresis is observed.

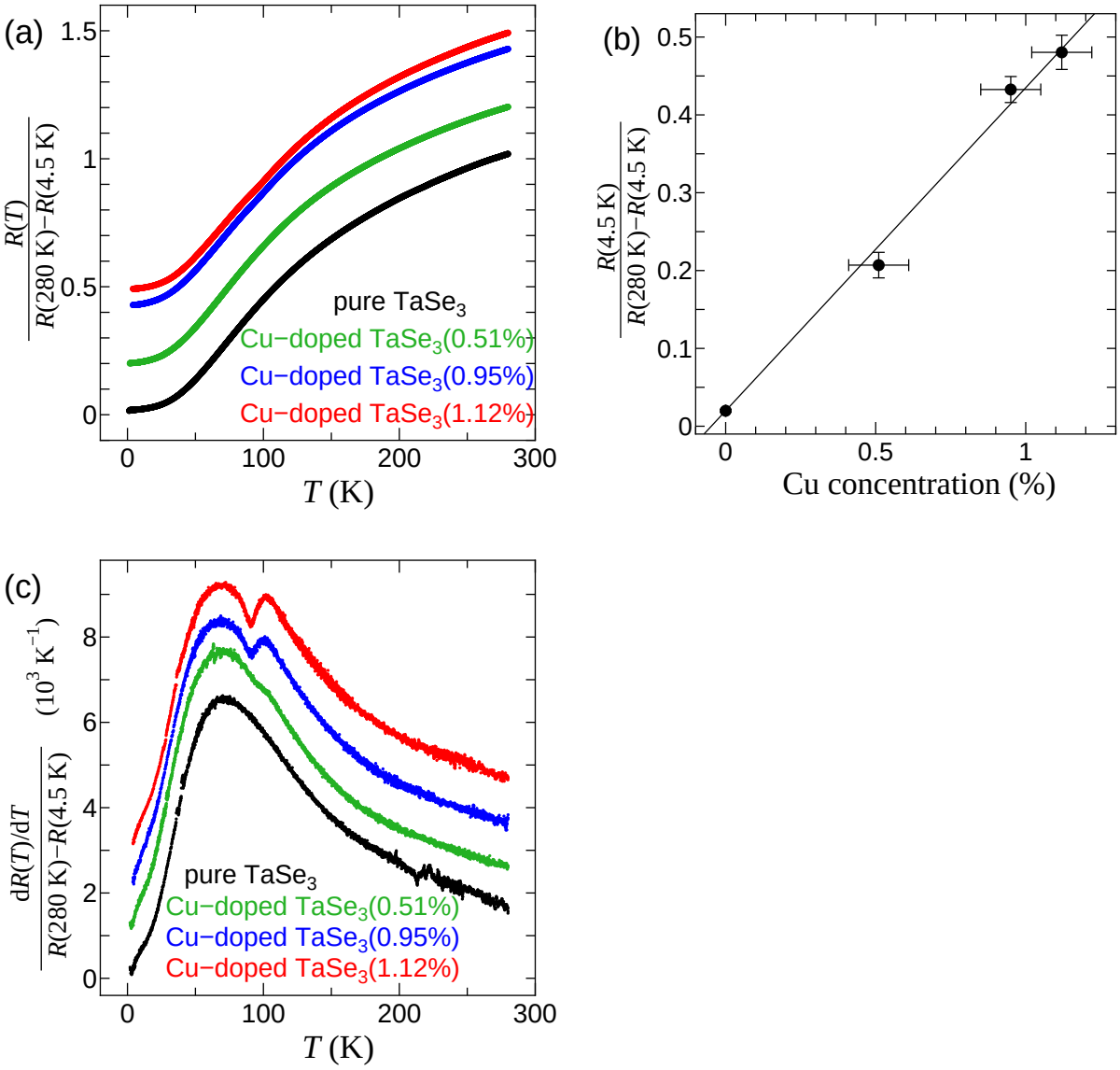

Figure 2.8: (a)The temperature dependence of the resistance normalized by the difference between the resistance at 4.5 K and that at 280 K of pure $TaSe_3$ and Cu-doped $TaSe_3$. (b)The resistance at 4.5 K normalized by the difference between the resistance at 4.5 K and that at 280 K as a function of Cu concentration. The average value is shown for each Cu concentration. (c)The temperature derivative of the normalized resistance in panel (a). The curves of Cu-doped $TaSe_3$ (0.51%), Cu-doped $TaSe_3$ (0.95%) and Cu-doped $TaSe_3$ (1.12%) are shifted vertically by 0.001, 0.002 and 0.003 K^{-1}, respectively.

2.4 Discussion

2.4.1 Change in the lattice parameters by Cu doping

The single-crystal XRD analysis shows that the lattice parameters have sample dependence and do not show Vegard's law clearly for increasing Cu concentration, as shown in Fig. 2.6. On the other hand, the RRR and the depth of the dip change systematically as the Cu concentration increases (see Fig. 2.7 and Fig. 2.8(c)). The beam-diameter used in the single-crystal XRD analysis is 0.15 mm and, as a result, the lattice parameters are determined as the average value over a local region of 0.15 mm in comparison with the resistance that is obtained as the average value over the region of 1–3 mm between the voltage terminals. Thus, the inhomogeneity in a single crystal may cause the sample dependence of the lattice parameters. However, the inhomogeneous distribution of Cu atoms is not the main cause because the sample dependence is observed not only in Cu-doped $TaSe_3$ but also in pure $TaSe_3$. The ideal value of the molar ratio of Se to Ta is 3. However, the actual molar ratio obtained using ICP-AES is 2.8–2.9 as shown in Table 2.2. This fact shows excess Ta atoms or Se vacancies. It is possible that there is inhomogeneous distribution of Ta and Se atoms in a single crystal which disturbs the lattice parameters and obscures the effect of Cu-doping, i.e., Vegard's law.

Therefore, we focus on the average value of the lattice parameter for each Cu concentration and discuss the change in lattice parameters by Cu-doping. As shown in Fig. 2.6, the average lattice parameter value tends to increase on the a-axis and c-axis (perpendicular to the chain axis) and tends to decrease on the b-axis (parallel to the chain axis) as the Cu concentration increases. The expansion of the a-axis and c-axis indicates that Cu atoms may be intercalated in the Van der Walls gap between chains. When the distance between chains is increased, and the chain axis is contracted, the dimensionality is expected to decrease because the overlap between wave functions perpendicular to the chain axis decreases and that in the chain axis direction increases. Therefore, the result of the

single-crystal XRD analysis implies that the change in lattice parameters caused by Cu-doping changes the Fermi surfaces from two-dimensional tunnel-like to one-dimensional flat. This would lead to a better nesting condition in Cu-doped $TaSe_3$ than in pure $TaSe_3$.

2.4.2 Change in the number of carriers by Cu doping

In addition, we can consider the number of carriers to be another physical quantity that is changed by Cu-doping. It is reported that the Cu atoms intercalated in the Van der Waals gap are donors contributing delocalized electrons at the Fermi level [16]. The Cu atoms in Cu-doped $TaSe_3$ are assumed to be intercalated in Van der Waals gaps, and contribute delocalized electrons. $TaSe_3$ is a semimetal with several Fermi surfaces which consist of a hole and an electron band [23]. In addition, the result of angle-resolved photoemission spectroscopy (ARPES) exhibits a high density of states near the Fermi level [31]. Thus, the density of states at the Fermi energy and the form of the Fermi surfaces are sensitive to a change in the number of carriers. It is possible that the change in the number of carriers caused by Cu-doping can also change the nesting condition although it does not necessarily get better.

2.4.3 "γ"-shaped dip

We find an anomalous sharp dip in the $\mathrm{d}R/\mathrm{d}T$ value in the temperature dependence of the $\mathrm{d}R/\mathrm{d}T$ of Cu-doped $TaSe_3$, which is never observed in that of pure $TaSe_3$, as shown in Fig. 2.8(c). The dip in $\mathrm{d}R/\mathrm{d}T$ is "γ" shaped with a sudden decrease and a narrow minimum. Thus, the dip suggests a sudden change in state. The emergence of a structural transition is suggested in pure $TaSe_3$ under uniaxial strain [35]. However, the sudden change in state in Cu-doped $TaSe_3$ would not be a first-order transition because we observe no thermal hysteresis.

We discuss how the resistance changes in the vicinity of the temperature where a dip in $\mathrm{d}R/\mathrm{d}T$ is present in Cu-doped $TaSe_3$. When the $\mathrm{d}R/\mathrm{d}T$ drops, the decrease in resistance caused by the decrease in temperature is suppressed. Thus, the resistance below the

onset temperature of the dip (102 K) is larger than the resistance extrapolated from the resistance-temperature curve above 102 K assuming that there is no dip in $\mathrm{d}R/\mathrm{d}T$. In summary, the dip in $\mathrm{d}R/\mathrm{d}T$ means a relative increase in resistance. MX_3 compounds ($NbSe_3$, TaS_3, NbS_3) other than $TaSe_3$ show anomalous increases in resistance at the CDW transition temperatures (T_{CDW}) because the whole or part of the Fermi surfaces disappears and the number of carriers decreases [24, 25, 26]. Therefore, the sudden change in state with a resistance increase in Cu-doped $TaSe_3$ is most likely to be a CDW formation although the resistance increase is relative.

We discuss the "γ"-shaped dip discovered in Cu-doped $TaSe_3$ by comparison with the temperature dependence of the $\mathrm{d}R/\mathrm{d}T$ in CDW conductors such as $NbSe_3$ [36], $DyTe_3$ [37], $HfTe_3$ [38] and $ZrTe_3$ [39]. These CDW conductors show the metallic temperature dependence of the resistance in the normal state above the T_{CDW}, and the resistance increase at the T_{CDW}. However, the temperature dependence of the resistance shows metallic behavior again at lower temperatures because the Fermi surfaces partly remain due to imperfect nesting. Although the magnitude of the resistance increase at T_{CDW} is different for the four CDW conductors, we find out a common dip in the $\mathrm{d}R/\mathrm{d}T$ value corresponding to the resistance increase as shown in Fig. 2.9 and Fig. 2.10. The $\mathrm{d}R/\mathrm{d}T$ is constant above the T_{CDW}, however with decreasing temperature, it falls sharply at the T_{CDW} and then starts to increase at the minimum point. At lower temperatures, it increases more gradually with a convex upward curvature and approaches a certain value. In short, the temperature dependence of the $\mathrm{d}R/\mathrm{d}T$ shows the common "γ"-shaped dip, indicating the universal law peculiar to the CDW formation. The law states that a CDW is formed with an energy gap opening on a Fermi surface. In the BCS theory on the CDW formation, the energy gap opens at T_{CDW} and grows obeying the temperature dependence of the gap function. The opening and growth of the CDW gap reduce the number of conducting carriers with decreasing temperature, leading to an increase in resistance near T_{CDW}, and at the same time the $\mathrm{d}R/\mathrm{d}T$ has a "γ"-shaped dip. Actually, we can reproduce the "γ"-

shaped dip by calculation as described in Appendix. This fact strongly indicates that the "γ"-shaped dip observed in Cu-doped $TaSe_3$ is caused by the CDW formation.

As shown in Fig. 2.8(c), the T_{dip} of Cu-doped $TaSe_3$ is about 91 K, which is lower than the T_{CDW} of the other MX_3 compounds (340 K in NbS_3 [26], 218 K in TaS_3 [29], and 145 K in $NbSe_3$ [24]). Originally pure $TaSe_3$ has two-dimensional Fermi surfaces [23], where the nesting condition is the worst in MX_3 compounds, thus it shows no CDW formation. Even if Fermi surfaces change and a CDW emerges in $TaSe_3$, the temperature at which a CDW forms is expected to be lower than the T_{CDW} of the other MX_3. Therefore, it will be consistent to assume that T_{dip} in Cu-doped $TaSe_3$ corresponds to the temperature of the CDW formation.

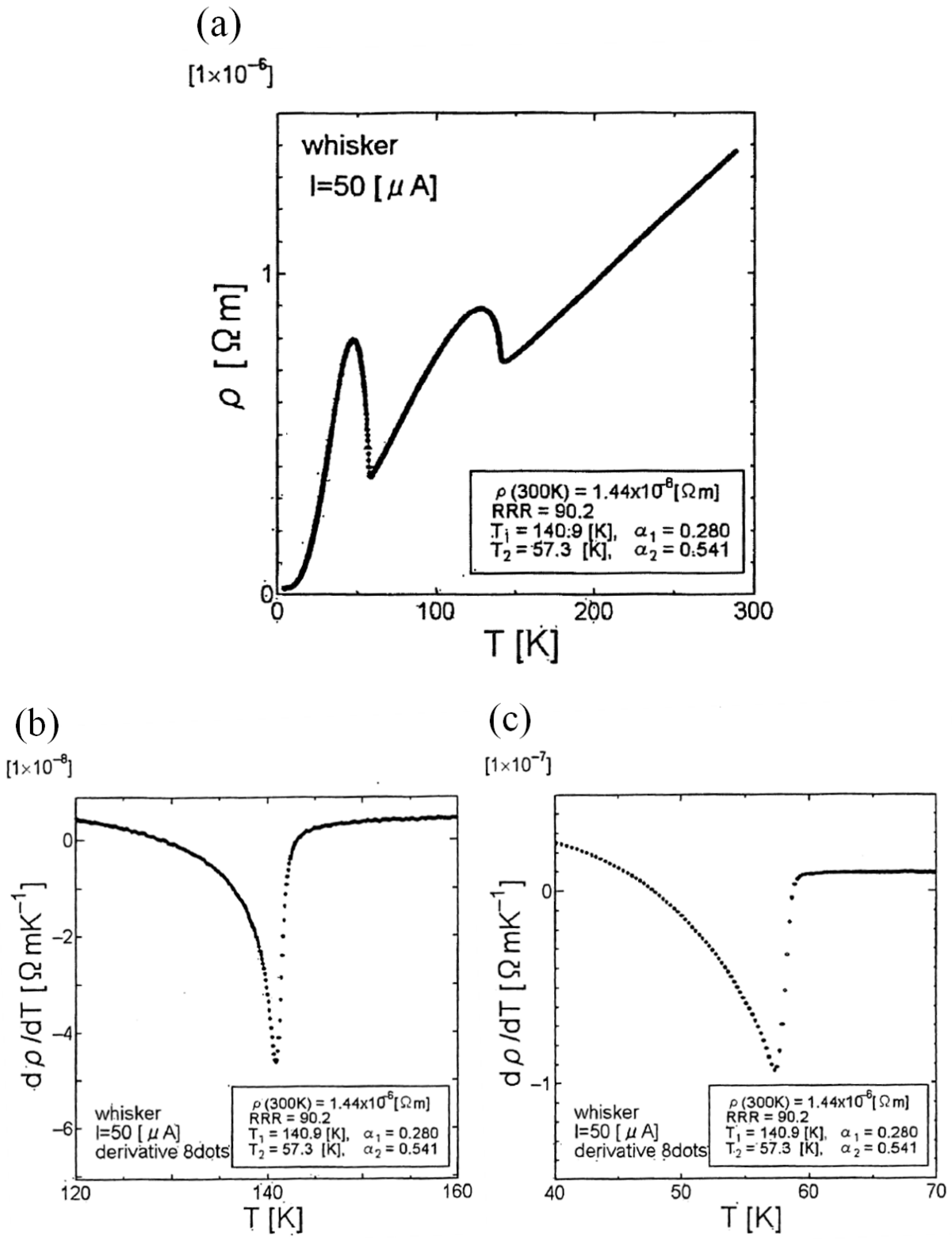

Figure 2.9: The temperature dependence of the resistance [(a)], its derivative for the upper CDW transition [(b)], and its derivative for the lower CDW transition [(c)] in a $NbSe_3$ whisker-crystal [36].

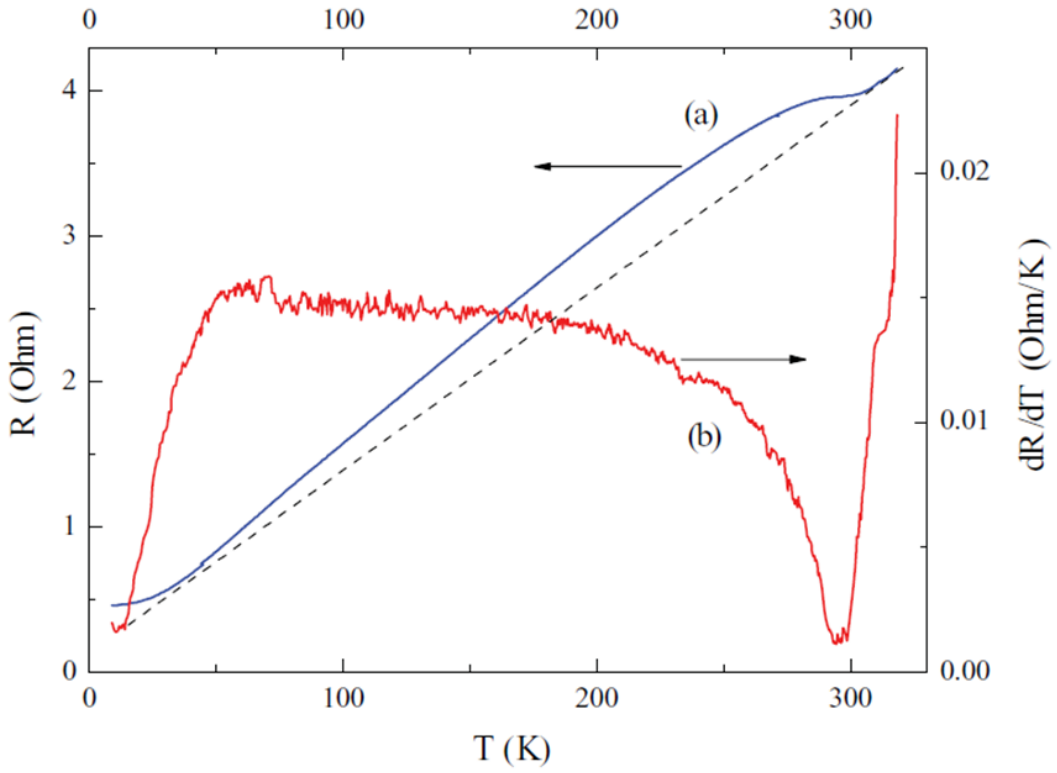

Figure 2.10: The temperature dependence of the resistance [curve (a)] and its derivative [curve (b)] in the $(a-c)$ plane of a $DyTe_3$ single-crystal [37]. The dotted line is the linear extrapolation of the resistance from above T_{CDW1}.

2.4.4 Emergence of a CDW

From the discussions above, the main features of the Cu-doped $TaSe_3$ system are summarized as follows: i)The change in the lattice parameters caused by Cu-doping may change the form of Fermi surfaces which leads to a better nesting condition. ii)The dip in dR/dT exhibits a sudden change in state with a relative increase in resistance. iii)The dip in dR/dT is "γ"-shaped and the same "γ"-shaped dip is commonly observed in many CDW conductors. Therefore, we can conclude that a CDW emerges by Cu doping in $TaSe_3$.

2.4.5 The CDW formation in the saddle-point mechanism

The above discussions about the CDW formation are based on the scenario of the Fermi surface nesting. However, the resistance increase seen in Cu-doped $TaSe_3$ is extremely small, suggesting alternative scenario for the CDW formation. Rice and Scott propose that Fermi surfaces with saddle points can be unstable against CDW formation [40]. In this model, only a relatively small area of Fermi surfaces disappears and a large area of those remains. Furthermore, the saddle points act as scattering sinks in the high-temperature phase above T_{CDW} and the conductivity can be enhanced at the T_{CDW} by the disappearance of the saddle points. As a result, the resistance increase due to the CDW formation is suppressed. Therefore, the present result suggests the possibility that the CDW formation is driven by the mechanism of Rice and Scott. Although the presence of saddle points in pure $TaSe_3$ is not mentioned by the result of the band calculation [23], the result of ARPES shows that there is the flat band region with a high density of states near the Fermi level in pure $TaSe_3$ [31]. This singularity might drive the CDW formation in Cu-doped $TaSe_3$. In order to verify this mechanism, the band structure of Cu-doped $TaSe_3$ has to be investigated by ARPES.

2.5 Conclusion

By measuring precisely the temperature dependence of the resistance in pure $TaSe_3$ and Cu-doped $TaSe_3$, we discovered an anomalous sharp dip in the temperature dependence of the temperature derivative of the resistance (dR/dT) in Cu-doped $TaSe_3$, which was never observed in pure $TaSe_3$. The dip suggests that there is a sudden change in state with a relative increase in resistance. Furthermore, the dip was "γ" shaped. We reveal that many CDW conductors commonly exhibit the same "γ"-shaped dip in dR/dT at the CDW transition temperature, which is a universal consequence of the opening and growth of a CDW gap on a Fermi surface. Furthermore, the result of the single-crystal X-ray diffraction (XRD) analysis implied that Cu doping increased the lattice parameter of the a-axis and c-axis and decreased that of the b-axis, leading to an improvement in the nesting condition. From the "γ"-shaped dip and the result of the single-crystal XRD analysis, we conclude that a CDW emerges by Cu doping in $TaSe_3$. Further studies are needed to obtain direct evidence of the CDW formation.

Chapter 3

Superconductivity in Cu-doped $TaSe_3$

3.1 Introduction

In chapter 2, we concluded that a CDW is induced by Cu doping in $TaSe_3$. On the other hand, $TaSe_3$ intrinsically exhibits the SC transition at about 2 K [22, 32, 33]. The SC transition curve in the temperature dependence of the resistivity is anisotropic as shown in Fig. 3.1 [41]. The resistivity parallel to the b-axis falls to zero at T_C, while that perpendicular to the b-axis exhibits a partial drop at T_C and a finite value even below T_C. Moreover, the diamagnetism induced by the SC transition is not observed in relation to the temperature dependence of the magnetic susceptibility shown in Fig. 3.2 [42]. From these results, it is considered that the SC of $TaSe_3$ is filamentary and composed of superconducting filaments parallel to the b-axis. Therefore, in this chapter, we investigated SC in Cu-doped $TaSe_3$ by measuring the temperature dependence of the resistance to clarify the effect of Cu doping on SC.

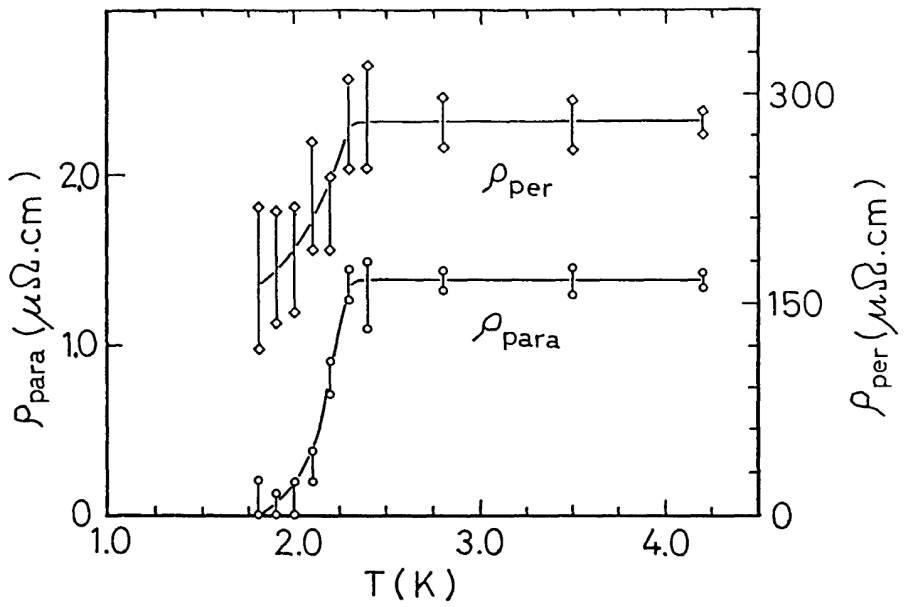

Figure 3.1: The temperature dependence of the resistivity along the parallel and perpendicular direction to the b-axis in $TaSe_3$ [41].

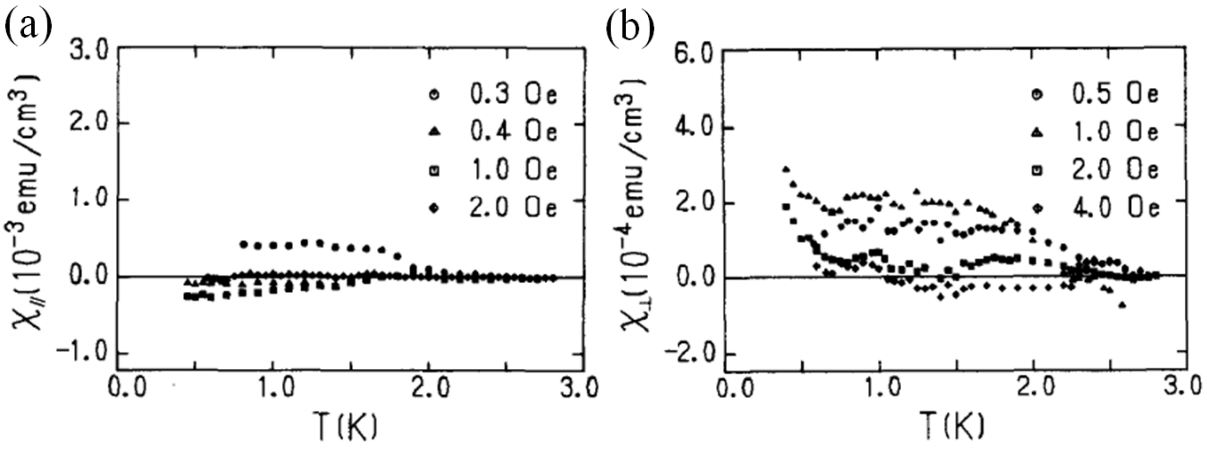

Figure 3.2: The temperature dependence of the susceptibility of $TaSe_3$ for several fields [42]. The data at 2.8 K are taken to be zero. (a)$H \parallel b$. The sample weight is 0.570 mg (7.05×10^{-5} cm^3, 6 mm length, 100 crystals).(b)$H \perp b$. The sample weight is 0.642 mg (7.94×10^{-5} cm^3, 3 mm length, 292 crystals). Demagnetization correction is not made.

3.2 Experimental

3.2.1 Synthesis of single crystals

We prepared single crystals of pure $TaSe_3$ and Cu-doped $TaSe_3$ synthesized by the vapor phase transport method in the same way as chapter 2. The growth temperature was 660°C as shown in Table. 3.1. The nominal value of Cu to Ta was 10% in Cu-doped $TaSe_3$. Crystals were ribbon-shaped with typical dimensions of $5\,\mu\mathrm{m} \times 10\,\mu\mathrm{m} \times 5\,\mathrm{mm}$. The ribbon plane is $(\bar{2}01)$ [22].

Table 3.1: The synthesis condition of pure $TaSe_3$ and Cu-doped $TaSe_3$.

Crystal	Nominal value of Cu (x)	Growth temperature
pure $TaSe_3$	0	660°C
Cu-doped $TaSe_3$	0.1	660°C

3.2.2 Resistance measurement

The temperature dependence of the resistance along the b-axis from 0.6 to 280 K was measured with a dc four-probe technique. We placed the current terminals and the voltage terminals as shown Fig 2.5. We measured the resistance while the samples were being warmed from 2 to 280 K over about 30 hours and from 0.6 to 2 K over about 30 minutes. The measurements from 0.6 to 2 K were performed applying static magnetic fields (0–80 mT) perpendicular to the ribbon plane as shown in Fig. 3.3 after the zero field cooling.

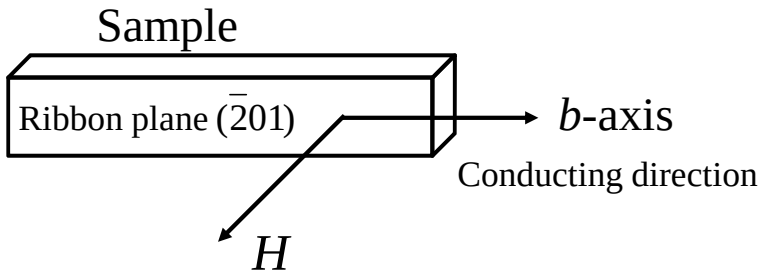

Figure 3.3: Schematic of the conduction direction and the magnetic field direction.

3.3 Results

3.3.1 Resistance measurement results from 2 K to 280 K

The resistance was measured for two samples of pure $TaSe_3$ and for four samples of Cu-doped $TaSe_3$. Figure 3.4 shows a typical result from 2 K to 280 K for pure $TaSe_3$ and Cu-doped $TaSe_3$. As shown in Fig. 3.4(a), all the samples showed that resistance had a metallic temperature dependence as with the results in Fig. 2.6. The residual resistance ratio ($RRR = R(280\ \mathrm{K})/R(4.5\ \mathrm{K})$) of Cu-doped $TaSe_3$ was smaller than that of pure $TaSe_3$. The normalized residual resistance ($R(4.5\ \mathrm{K})/(R(280\ \mathrm{K}) - R(4.5\ \mathrm{K}))$) of Cu-doped $TaSe_3$ was larger than that of pure $TaSe_3$ as shown in Fig. 3.4(b). The characteristics of all the samples are summarized in Table 3.2. As shown in Fig. 2.7(a, b), Matthiessen's rule holds for the Cu-doped $TaSe_3$ system, and the normalized residual resistance increases almost as a linear function of the Cu concentration determined by inductively coupled plasma atomic emission spectroscopy (ICP-AES). We obtained the empirical formula

$$y = 0.41x + 0.02, \tag{3.1}$$

where y is the normalized residual resistance and x is the Cu concentration [%]. Using this empirical formula, we estimated the Cu concentration of each Cu-doped $TaSe_3$ sample from the normalized residual resistance that we observed in this chapter (Table 3.2). The estimated Cu concentration varied in the 0.78–1.04% range among samples from the same batch. As shown in Fig. 3.4(c), a "γ"-shaped dip in $\mathrm{d}R/\mathrm{d}T$ was observed at $\sim$91 K in Cu-doped $TaSe_3$. The dip size tended to increase with increasing estimated Cu concentration, which is consistent with the result in Fig. 2.7(c).

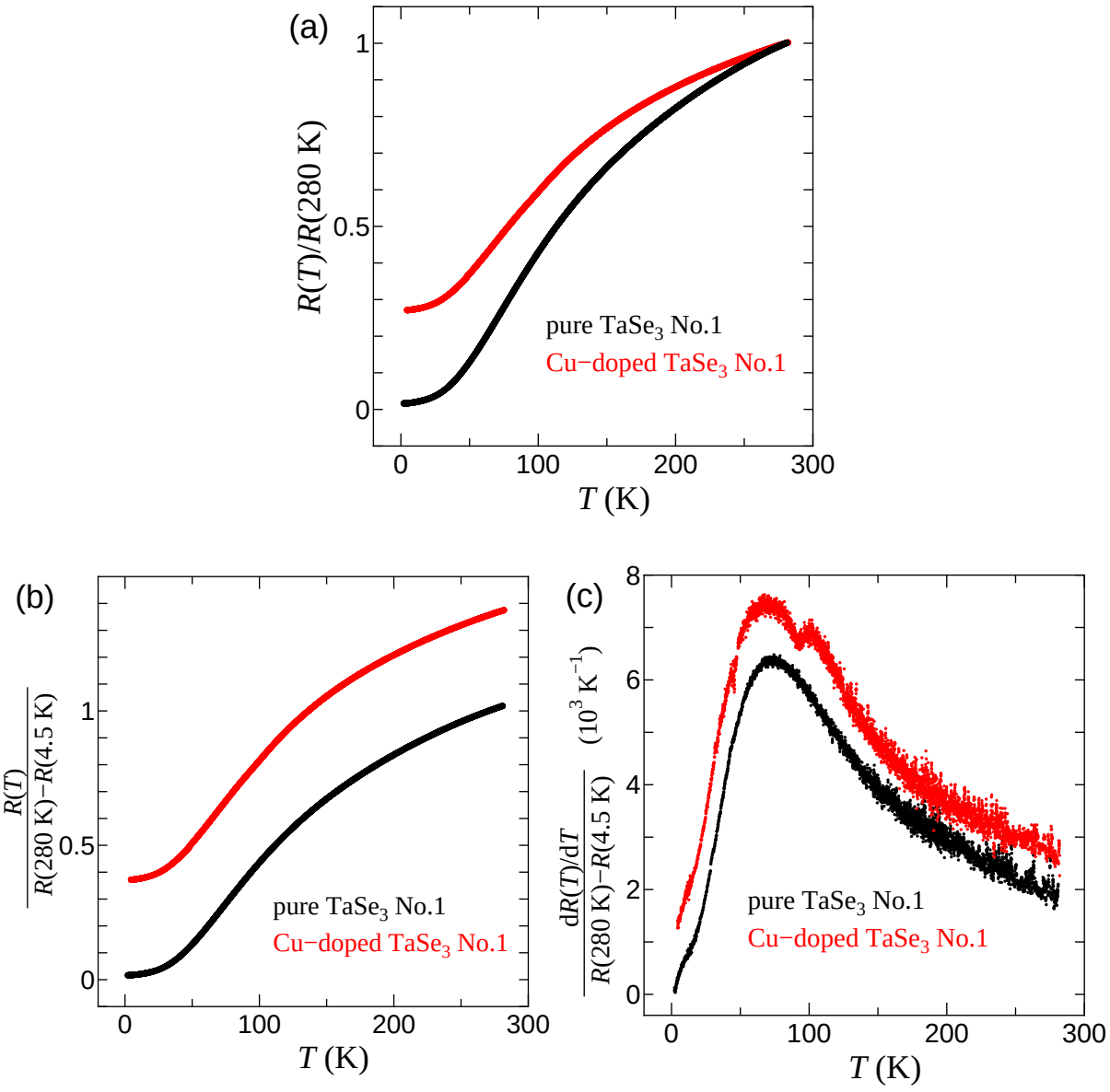

Figure 3.4: Typical resistance measurement results for pure $TaSe_3$ and Cu-doped $TaSe_3$ from 2 K to 280 K. The normalization was in accordance with Fig. 2.7 and Fig. 2.8. (a) The temperature dependence of the resistance normalized by the resistance at 280 K. (b) The temperature dependence of the resistance normalized by the difference between the resistances at 280 K and 4.5 K. (c) The temperature derivative of the normalized resistance in panel (b). The curve of Cu-doped $TaSe_3$ is shifted vertically by 0.001 K^{-1}.

Table 3.2: Characteristics of samples of pure $TaSe_3$ and Cu-doped $TaSe_3$.

Sample	$R(4.5\,\mathrm{K})$ [Ω]	$R(280\,\mathrm{K})$ [Ω]	RRR	y^*	x [%]**	T_C [K]
pure $TaSe_3$ No.1	2.278	135.391	59.43	0.01711		1.72
pure $TaSe_3$ No.2	1.385	81.256	58.67	0.01734		1.54
Cu-doped $TaSe_3$ No.1	5.613	20.695	3.687	0.3722	0.86	$(1.6)^{***}$, 1.07
Cu-doped $TaSe_3$ No.2	67.05	217.22	3.240	0.4465	1.04	$(1.5)^{***}$, 1.14
Cu-doped $TaSe_3$ No.3	9.908	37.116	3.746	0.3642	0.83	1.51, 1.15
Cu-doped $TaSe_3$ No.4	11.77	46.58	3.957	0.3382	0.78	1.69

$*y$ is the normalized residual resistance defined as $R(4.5\,\mathrm{K}) \,/\, (R(280\,\mathrm{K}) - R(4.5\,\mathrm{K}))$.
$**x$ is Cu concentration estimated from y.
$***$Approximate temperature at which the resistance begins to decrease.

3.3.2 Resistance measurement results from 0.6 K to 2 K

Figure 3.5 shows the temperature dependence of the resistance of pure $TaSe_3$ and Cu-doped $TaSe_3$ from 0.6 K to 2 K. All the samples of pure $TaSe_3$ and Cu-doped $TaSe_3$ exhibited a sharp drop in resistance due to the SC transition below 1.7 K. As shown in Fig. 3.5(a), the SC transition exhibited electric current dependence, which matches the results of previous studies [42, 43]. With increasing current, the onset of the SC transition did not move while the offset shifted to the low-temperature side. Therefore, we determine T_C as defined in Fig. 3.5(a) from the SC transition curve observed for the smallest electric current in this measurement. The SC transition temperatures (T_Cs) are summarized in Table 3.2. Pure $TaSe_3$ samples No.1 and 2 exhibited a one-step SC transition with a T_C of 1.54 K and 1.72 K, respectively. In Cu-doped $TaSe_3$ samples No.1 and 2, the resistance began to decrease at ∼1.6 K and 1.5 K, respectively, as shown in the inset of Fig. 3.5(c), and droped mostly at 1.07 K and 1.14 K. Sample No.3 exhibited a two-step SC transition with T_Cs of 1.51 K and 1.15 K. Sample No.4 exhibited a one-step SC transition with a T_C of ∼1.69 K. The ratio of the value of the drop in resistance at ∼1.1 K to the normal-state resistance is ∼0.99 for No.1, ∼0.93 for No.2, ∼0.63 for No.3, and 0 for No.4. The samples were No. 4, 3, 1 and 2 in ascending order of Cu concentration as shown in Table 3.2. Thus, the ratio tended to be higher with increasing Cu concentration.

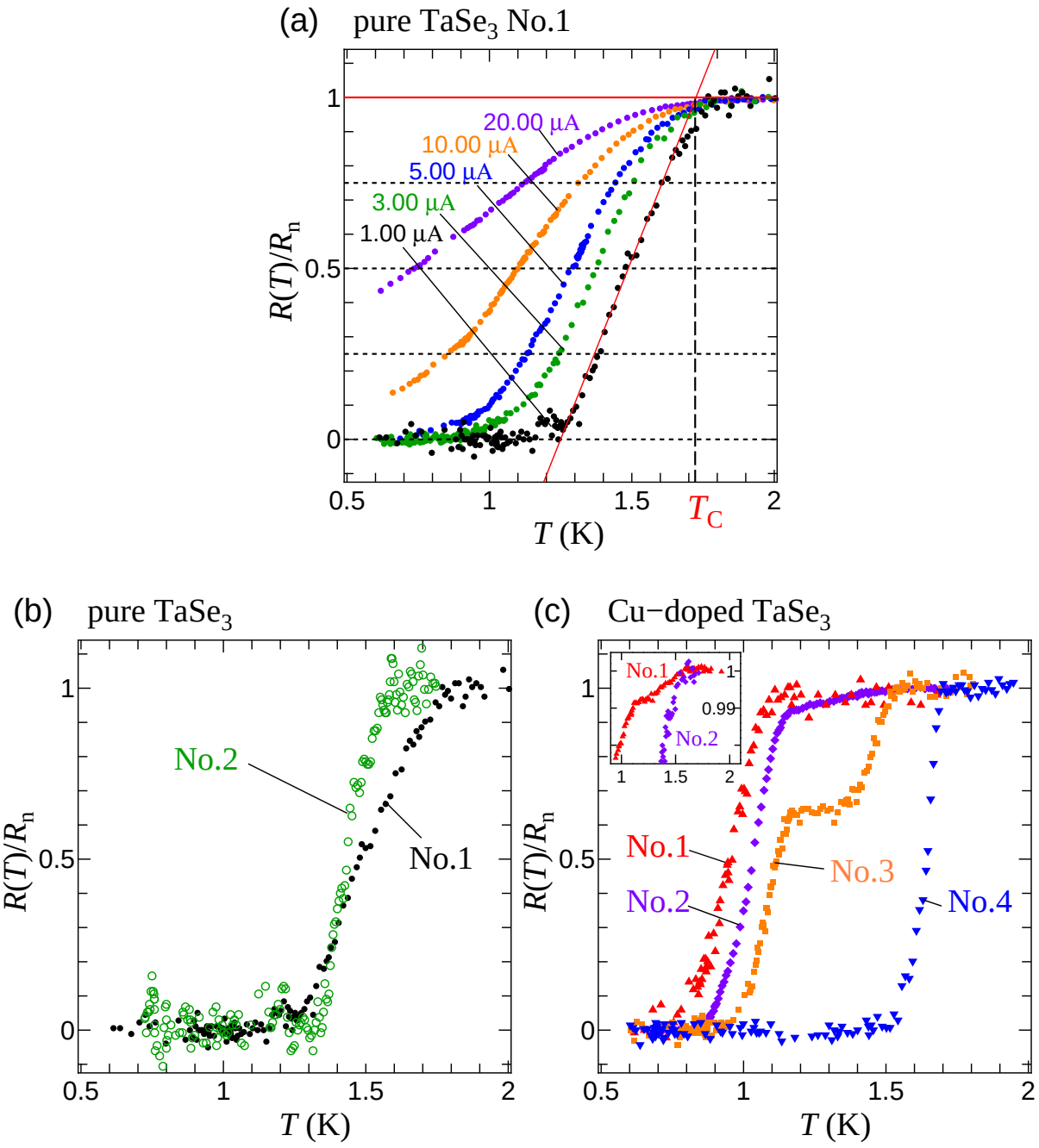

Figure 3.5: The temperature dependence of the resistance from 0.6 K to 2 K normalized by the normal-state resistance (R_n) of pure $TaSe_3$ and Cu-doped $TaSe_3$. (a) The SC transition curves for various electric currents of pure $TaSe_3$ sample No.1, and the definition of T_C. We define T_C as the intersection between a straight line fitted to the data of $R = 0.25R_n$–$0.75R_n$ and the straight line of $R = R_n$. (b) Pure $TaSe_3$ No.1 ($I = 1.00\,\mu$A) and No.2 ($I = 0.40\,\mu$A). (c) Cu-doped $TaSe_3$ No.1 ($I = 0.30\,\mu$A), No.2 ($I = 0.30\,\mu$A), No.3 ($I = 0.30\,\mu$A), and No.4 ($I = 0.30\,\mu$A). The inset is an enlarged view for Cu-doped $TaSe_3$ No.1 and 2. The data of sample No.1 in the inset is for $I = 20.00\,\mu$A, whose scattering is smaller than that for $I = 0.30\,\mu$A.

3.3.3 The location dependence of the superconductivity transition

Cu-doped $TaSe_3$ sample No.3 exhibited a two-step SC transition. To investigate the cause of this result, we measured the temperature dependence of the resistance between the current terminals, and the resistance between a current terminal and a voltage terminal with a dc two-probe measurement. Figure 3.6(a) shows the results. Sharp drops in resistance due to the SC transition were clearly observed between any pair of terminals, although the resistance measured with a two-probe method did not become zero because of the resistances due to contacts and lead lines ($\sim$ 240 Ω). The SC transition differed according to the combination of terminals, showing that various regions with different T_Cs are aligned in series in the b-axis direction as shown in Fig. 3.6(b). Thus, the two-step SC transition of sample No.3 was caused by the coexistence of two regions with T_Cs of $\sim$1.6 K and $\sim$1.1 K between voltage terminals, and the value of the drop in resistance for each T_C corresponded to the size of the region with the T_C. Cu-doped $TaSe_3$ samples No.1 and 2 also exhibited a non-single SC transition, where the resistance began to decrease at $\sim$1.6 K and droped mostly at $\sim$1.1 K. Therefore, two regions with T_Cs of $\sim$1.6 K and $\sim$1.1 K would coexist and the region with the T_C of $\sim$1.1 K would occupy most of these samples.

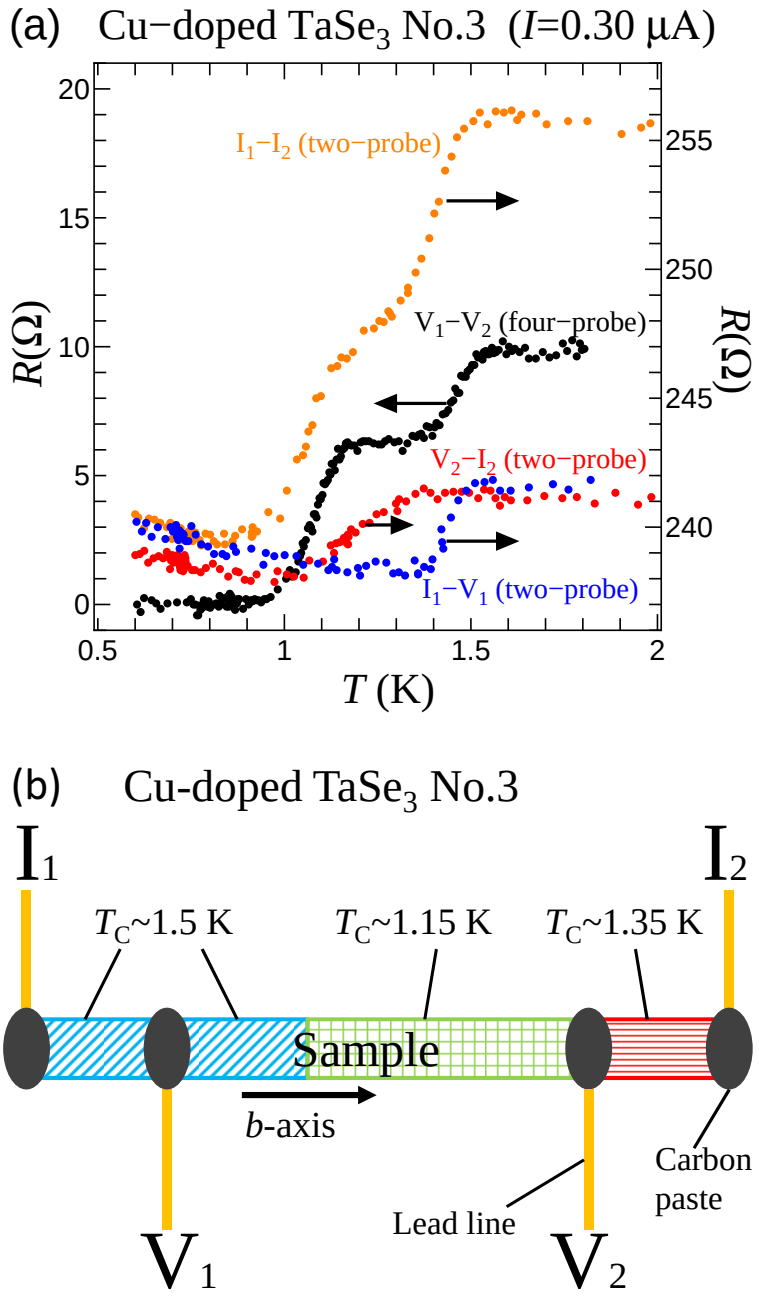

Figure 3.6: (a) The temperature dependence of the resistance between the voltage terminals, between the current terminals, and between a current terminal and a voltage terminal in Cu-doped $TaSe_3$ sample No.3. (b) Schematic of spatial distribution of T_C in Cu-doped $TaSe_3$ sample No.3 derived from panel 4(a). However, the distribution of the regions with the T_Cs of ∼1.6 K and ∼1.15 K between the voltage terminals is deduced.

3.3.4 The superconductivity transition under static magnetic fields

Figure 3.7(a) shows a typical temperature dependence of the resistance from 0.6 K to 2 K under various magnetic fields perpendicular to the ribbon plane ($\bar{2}01$). As the magnetic field increased, the SC transition curve shifted to the low-temperature side. Figure 3.7(b) shows the temperature dependence of the upper critical field (H_{C2}) perpendicular to the ribbon plane ($\bar{2}01$) of pure $TaSe_3$ and Cu-doped $TaSe_3$. As the temperature decreased, H_{C2} of pure $TaSe_3$ sample No.1 increased with an upward curvature, and H_{C2} of pure $TaSe_3$ sample No.2 increased with temperature dependence as a linear function near T_C and with an upward curvature at low temperatures. H_{C2} of Cu-doped $TaSe_3$ sample No.2 increased with an upward curvature, and H_{C2} of Cu-doped $TaSe_3$ sample No.4 increased with a downward curvature near T_C of $\sim$1.6 K and with an upward curvature at low temperatures. In Cu-doped $TaSe_3$ sample No.3, H_{C2} for the first-step SC transition exhibited an upward curvature and that for the second-step SC transition exhibited a slightly downward curvature. The curvature for Cu-doped $TaSe_3$ sample No.1 was unknown because there were only two points.

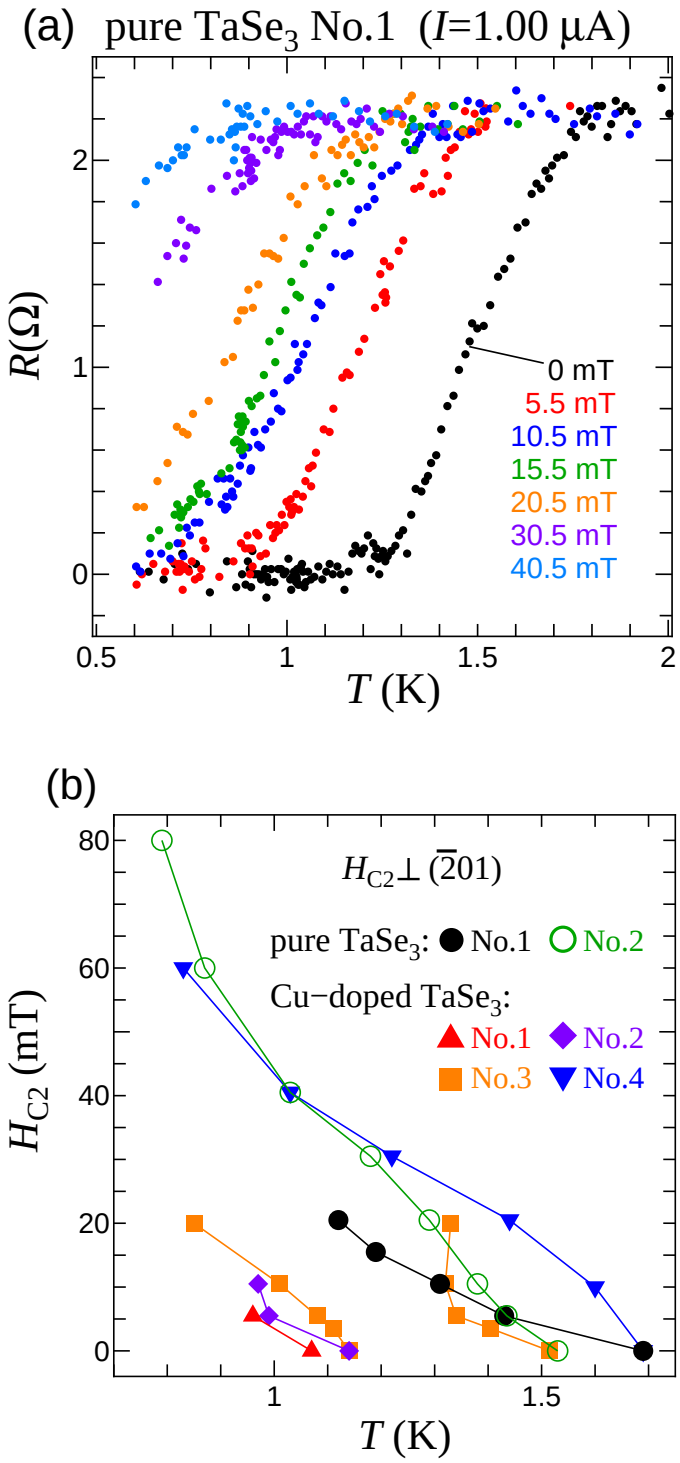

Figure 3.7: (a) The temperature dependence of the resistance of pure $TaSe_3$ sample No.1 from 0.6 K to 2 K under various magnetic fields perpendicular to the ribbon plane $(\bar{2}01)$. (b) The temperature dependence of H_{C2} perpendicular to the ribbon plane $(\bar{2}01)$ of pure $TaSe_3$ and Cu-doped $TaSe_3$. We define H_{C2} for the T_C shown in Fig. 3.5(a).

3.4 Discussion

3.4.1 Model of the superconducting filament structure

The SC of $TaSe_3$ is filamentary, and adjacent superconducting filaments are coupled to each other by the Josephson effect [41, 42]. A superconducting filament is considered to be composed of multiple $TaSe_3$ chains. In our result, pure $TaSe_3$ exhibits a one-step SC transition at ∼1.6 K (See Fig. 3.5(b)). As shown in Fig. 3.8(a), superconducting filaments with a T_C of ∼1.6 K parallel to the *b*-axis are bundled in pure $TaSe_3$. On the other hand, Cu-doped $TaSe_3$ samples No.1, 2 and 3 with higher Cu concentrations exhibit a coexistence of two regions with T_Cs of ∼1.6 K, ∼1.1 K, and the region with the T_C of ∼1.1 K tends to be larger with increasing Cu concentration (Fig. 3.5(c) and Fig. 3.6). This result indicates that the Cu doping suppresses the SC of $TaSe_3$. However, Cu-doped $TaSe_3$ sample No.4 with the smallest Cu concentration exhibits a one-step SC transition at ∼1.6 K as with pure $TaSe_3$ (Fig. 3.5(c)). Moreover, there is a region with a T_C of ∼1.6 K in Cu-doped $TaSe_3$ samples No.1, 2 and 3. The Cu concentrations of the present four Cu-doped $TaSe_3$ samples (Table 3.2) are lower than that of the Cu-doped $TaSe_3$ sample with the highest Cu concentration observed in chapter 2 (Table 2.2). The lower Cu concentrations and the location dependence of the T_C in a sample (Fig. 3.6) suggest that there are some areas that no Cu atom enters in a sample and the area increases with decreasing Cu concentration. In addition, the suppression of SC by a Cu atom might be limited within a SC filament rather than the entire sample because the SC of $TaSe_3$ is filamentary. Therefore, it is believed that, in a sample, there are filaments where Cu atoms enter and SC is suppressed, and filaments where Cu atoms do not enter and SC is not suppressed. If there is a superconducting path composed of superconducting filaments where no suppression remain, the partial suppression of SC cannot be observed by measuring the resistance because the electric current flows through the superconducting path with zero resistance. Therefore, as regards the invariant SC transition in Cu-doped

$TaSe_3$ sample No.4 and the region where T_C does not change in samples No.1, 2 and 3, it can be interpreted that more than one superconducting path with a T_C of ∼1.6 K remains as shown in Fig. 3.8(b, c). Inhomogeneous SC as observed in Cu-doped $TaSe_3$ has been extensively studied theoretically and experimentally in other systems [44, 45, 46].

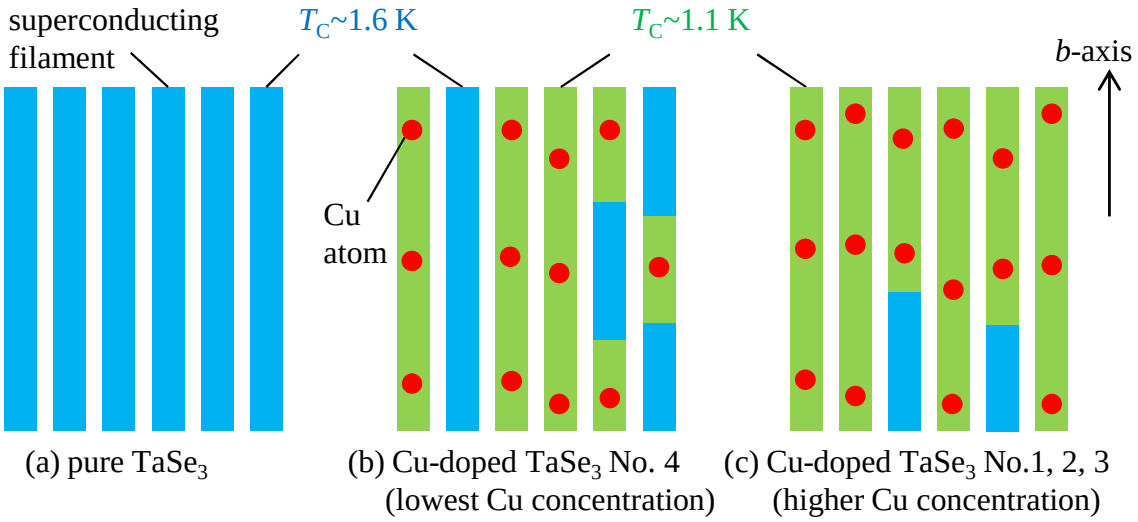

Figure 3.8: Model of the SC filament structures of pure $TaSe_3$ and Cu-doped $TaSe_3$. The T_C of suppressed SC is represented by 1.1 K overall.

3.4.2 Change in the H_{C2}-temperature curve by Cu doping

We compare the temperature dependence of H_{C2} for pure $TaSe_3$ and Cu-doped $TaSe_3$. H_{C2} is derived from the Pauli paramagnetic and orbital effects. However, the Pauli paramagnetic limit will not matter in the present range of magnetic fields (0–80 mT). Considering orbital effects based on the Ginzburg-Landau (GL) theory, the temperature dependence of the H_{C2} of bulk superconductors is expressed as

$$H_{C2}(t) = H_{C2}(0)\frac{1-t^2}{1+t^2}, \tag{3.2}$$

where t is the normalized temperature ($t = T/T_C$). However, the temperature dependence of the H_{C2} of pure $TaSe_3$ and Cu-doped $TaSe_3$ (Fig. 3.7(b)) cannot be expressed by eq. 3.2. Thus, we require a theoretical model that considers the special feature of the SC of $TaSe_3$, namely filamentary SC. According to the GL theory of filamentary SC proposed by L. A. Turkevich and R. A. Klemm (the TK theory), the H_{C2} for Josephson-coupled superconducting filaments increases with an upward curvature as temperature decreases [47]. On the other hand, the H_{C2} for decoupled superconducting filaments increases with a downward curvature. The temperature dependence of the H_{C2} exhibits an upward curvature in the two pure $TaSe_3$ samples (Fig. 3.7(b)). From the TK theory, this result implies the Josephson coupling of superconducting filaments. Even in our model, as shown in Fig. 3.8(a), the SC of pure $TaSe_3$ is composed of coupled superconducting filaments with the same T_C. In contrast, the temperature dependence of the H_{C2} exhibits a downward curvature near a T_C of $\sim$1.6 K in Cu-doped $TaSe_3$ sample No.4 with the same SC transition as pure $TaSe_3$. Thus, according to the TK theory, the superconducting filaments are decoupled near 1.6 K in this sample. This result is consistent with our model shown in Fig. 3.8(b) where the superconducting filaments with a T_C of $\sim$1.6 K are sparse. In other Cu-doped $TaSe_3$ samples No.2 and 3, the temperature dependence of the H_{C2} exhibits an upward curvature or a downward curvature. Cu doping results in superconducting filaments with different T_Cs being mixed in a sample as shown in

Fig. 3.8(c). As a result, there are regions where superconducting filaments with the same T_C are adjacent and coupled, and regions where superconducting filaments with different T_Cs are adjacent and not coupled. This complex configuration of superconducting filaments might lead to the complex sample dependence of the H_{C2}-temperature curve.

3.5 Conclusion

We investigated SC in Cu-doped $TaSe_3$ by measuring the temperature dependence of the resistance. The Cu-doped $TaSe_3$ sample with the smallest Cu concentration exhibited a one-step SC transition with a T_C of $\sim$1.6 K as well as pure $TaSe_3$. On the other hand, those with larger Cu concentrations exhibited a two-step SC transition with T_Cs of $\sim$1.6 K and $\sim$1.1 K, or a non-single SC transition where the resistance began to decrease at $\sim$1.6 K and droped mostly at $\sim$1.1 K. The value of the drop in resistance at $\sim$1.1 K tended to expand with increasing Cu concentration. The location dependence of the SC transition showed that the two-step SC transition and the non-single SC transition are caused by the coexistence of two regions with T_Cs of $\sim$1.6 K and $\sim$1.1 K aligned in series in the b-axis direction in a sample. The temperature dependence of the H_{C2} of Cu-doped $TaSe_3$ exhibits upward curvature or downward curvature while that of pure $TaSe_3$ exhibits upward curvature. From these SC results and the fact that the SC in $TaSe_3$ is filamentary, we conclude that SC is suppressed locally by Cu doping in all Cu-doped $TaSe_3$ samples.

Chapter 4

Further discussion

4.1 Competitive relationship between superconductivity and the induced CDW

From the results in chapter 2, we found that a CDW emerges in Cu-doped $TaSe_3$. On the other hand, the SC intrinsically present in $TaSe_3$ is suppressed by Cu doping from the results in chapter 3. Hence, the induced CDW and SC would be in a competitive relationship in Cu-doped $TaSe_3$.

4.2 Short-range order of the induced CDW

We discuss the the induced CDW in Cu-doped $TaSe_3$ because the CDW property is important when discussing the relationship between SC and CDW. The SC suppression of $TaSe_3$ is local in the filament where Cu atoms enter as shown in Fig. 3.8. Therefore, it is possible that there is no coherent CDW in the entire sample, but CDWs exist locally.

From the viewpoint of the locality of CDWs, we reconsider the resistance anomaly results, that is, the "γ"-shaped dip in $\mathrm{d}R/\mathrm{d}T$ due to the CDW formation in Cu-doped $TaSe_3$. Conventional CDW materials such as $NbSe_3$, TaS_3 and NbS_3 exibit anomalous increases in resistance at the T_{CDW}) because all or part of the Fermi surface disappears and the number of carriers decreases [24, 25, 26]. On the other hand, the resistance anomaly of Cu-doped $TaSe_3$ is extremely small as shown in Fig. 2.8(c). This result for Cu-doped $TaSe_3$ may arise because of the locality of the existence of the CDWs. In fact, in Cu_xTiSe_2, no signal due to the formation of short-range order CDWs is observed in the temperature dependence of the resistance [5].

Moreover, a comparison of the "γ"-shaped dips of Cu-doped $TaSe_3$ samples with different Cu concentrations shows that the dip size increases with increasing Cu concentration while the temperature at which the dip appears is almost constant as shown in Fig. 2.8(c). The dip size corresponds to the area of the reduced Fermi surface, and the dip appearance temperature corresponds to T_{CDW}. The relationship between the dip size and the dip appearance temperature appears to contradict the prediction for long-range order CDW with the mean-field theory, which shows a positive correlation between the area of the reduced Fermi surface and T_{CDW}. However, if the induced CDWs have short-range order in the vicinity of Cu atoms and the size of a CDW is shorter than the distance between Cu atoms, we can interpret the conflicting result mentioned above consistently, namely that the size increases with increasing Cu concentration because the number of short-range order CDWs increases, while the appearance temperature is constant because the state of each short-range order CDW is unchanged.

Here, we estimate the size of short-range order CDWs from a simple calculation of the distance between Cu atoms. The volume of a unit cell of $TaSe_3$ is estimated to be $\sim$0.34 nm^3 from the lattice parameters determined in this study, and a unit cell contains four Ta atoms. In addition, the Cu concentration of Cu-doped $TaSe_3$ is at most 1%. Hence, if Cu atoms enter a crystal evenly, each Cu atom enters a space of $\sim$8.5 ($= 0.34/(4 \times 0.01)$) nm^3 and the distance between adjacent Cu atoms is estimated to be $\sim$2 nm. Therefore, the CDW size must be shorter than $\sim$2 nm.

4.3 The effect of the pinning of CDWs on the relationship between superconductivity and short-range order CDWs

The estimated size of the CDWs in Cu-doped $TaSe_3$ is on a nanometer-scale and comparable to the size of the short-range order CDWs in Cu_xTiSe_2 [16]. In Cu_xTiSe_2, the short-range order CDWs do not compete with the SC transition. On the other hand, our results suggest that short-range order CDWs compete with SC in Cu-doped $TaSe_3$. One of differences between the two materials is that the CDWs form on Cu atoms in Cu-doped $TaSe_3$ while the CDW is suppressed in the area where Cu atoms enter in Cu_xTiSe_2 [16]. Generally, when there is an impurity, a CDW is pinned by that impurity [48]. Hence, the CDWs in Cu-doped $TaSe_3$ would be harder to move than those in Cu_xTiSe_2. Moreover, in Cu_xTiSe_2, the modulation period of the CDWs changes from commensurate to incommensurate at the Cu concentration where the SC phase emerges [17]. In general, a commensurate CDW is harder to move than an incommensurate CDW [48]. Therefore, CDWs may compete with SC when CDWs are hard to move due to impurity pinning or commensurate pinning. We should note that, when discussing the relationship between SC and another electron ordering which is periodically modulated, there is a case where whether the electron ordering is static or dynamic is important [49].

Chapter 5

Genaral conclusion

We measured precisely the temperature dependence of the resistance of Cu-doped $TaSe_3$. As a result, we discovered a "γ"-shaped dip in dR/dT at $\sim$91 K in Cu-doped $TaSe_3$, which was never observed in pure $TaSe_3$. The dip suggests that there is a sudden change in state with a relative increase in resistance. We reveal that many CDW conductors commonly exhibit the same "γ"-shaped dip in dR/dT at the CDW transition temperature, which is a universal consequence of the opening and growth of a CDW gap on a Fermi surface. The result of the single-crystal XRD analysis implied that Cu doping increased the lattice parameter of the a-axis and c-axis and decreased that of the b-axis, leading to an improvement in the nesting condition. Based on the "γ"-shaped dip and the result of the single-crystal XRD analysis, we conclude that a CDW emerges by Cu-doping in $TaSe_3$.

We investigated the effect of Cu doping on SC in Cu-doped $TaSe_3$. In pure $TaSe_3$ and Cu-doped $TaSe_3$ sample with the smallest Cu concentration, the SC transition has a step with a T_C of $\sim$1.6 K. On the other hand, in Cu-doped samples with larger Cu concentrations exhibited a two-step SC transition with T_Cs of $\sim$1.6 K and $\sim$1.1 K, or a non-single SC transition where the resistance began to decrease at $\sim$1.6 K and droped mostly at $\sim$1.1 K. The ratio of the drop in resistance at $\sim$1.1 K tended to expand with increasing Cu concentration. The location dependence of the SC transition in a sample showed that the two-step SC transition and the non-single SC transition are caused by the

coexistence of two regions with T_Cs of ∼1.6 K and ∼1.1 K aligned in series in the b-axis direction. The H_{C2}-temperature curve of Cu-doped $TaSe_3$ exhibits upward curvature or downward curvature while that of pure $TaSe_3$ exhibits upward curvature. From these SC results and the fact that the SC in $TaSe_3$ is filamentary, we conclude that SC is suppressed locally by Cu doping.

The above results show that a CDW is induced while SC is suppressed in Cu-doped $TaSe_3$. Therefore, the induced CDW and SC are in a competitive relationship.

The locality of SC suppression suggests that the induced CDWs are local. The increase in resistance due to the CDW transition was extremely small. In addition, as the Cu concentration increased, the size of the "γ"-shaped dip was enhanced but the temperature at which the dip appeared hardly changed. These results of the induced CDW transition can consistently be interpreted from the short-range order which the induced CDWs in the vicinity of Cu atoms have.

From all the discussions, we conclude that the induced short-range order CDWs and SC are in a competitive relationship in Cu-doped $TaSe_3$. On the other hand, it was previously reported that short-range order CDWs and SC do not compete in Cu_xTiSe_2 where SC is induced in a CDW material. By comparing the detailed experimental results of these two materials, we will clarify the physics that defines the relationship between short-range order CDWs and SC.

Table 5.1: The relationship between SC and CDW.

①SC and CDW intrinsically exist in a material (e.g.: $ZrTe_3$ under pressure [14])	Competition
②SC is induced in a CDW material (e.g.: Ta_xNbSe_3 [15], Cu_xTiSe_3 [5, 16, 17])	Competition (Long-range order CDW) Non-competition (Short-range order CDW)
③CDW is induced in a SC material (Cu-doped $TaSe_3$ in this study)	Competition (Short-range order CDW)

Appendix

Reproduction of "γ"-shaped dip by calculation

We reproduce that CDW conductor exhibits a "γ"-shaped dip in the temperature derivative of the resistivity ($\mathrm{d}\rho(T)/\mathrm{d}T$) at T_{CDW} by calculation. In the Drude theory, the resistivity ($\rho(T)$) of metal is expressed as

$$\rho(T) = \frac{m^*}{n(T)e^2\tau(T)}, \tag{5.1}$$

where T is temperature, m^* is the effective mass of conduction electron, $n(T)$ is the density of conduction electrons, e is the elementary charge, and $\tau(T)$ is the mean free time. We assume that $n(T)$ is constant above T_{CDW} and depends on temperature due to CDW gap formation below T_{CDW}. Moreover, considering impurity scattering and phonon scattering as the scattering mechanism of conduction electrons, $1/\tau(T)$ in both the normal state and the CDW state is assumed to be expressed by the following equation.

$$\frac{1}{\tau(T)} = \frac{1}{\tau_{\mathrm{i}}} + \frac{1}{\tau_{\mathrm{p}}(T)} = \frac{1}{\tau_{\mathrm{i}}} + \frac{T}{a}. \tag{5.2}$$

τ_{i} is the mean free time for impurity scattering and does not depend on temperature. τ_{p} is that for phonon scattering, which is proportional to the inverse of temperature. a is a constant. Substituting Eq. 5.2 into Eq. 5.1, we obtain the equation

$$\rho(T) = \frac{m^*}{n(T)e^2}\left(\frac{1}{\tau_{\mathrm{i}}} + \frac{T}{a}\right). \tag{5.3}$$

First, we consider the normal state above T_{CDW}. In the normal state, $n(T)$ is expressed as

$$n(T) = n_n, \qquad (n_n : \text{const.}, \quad T > T_{\mathrm{CDW}}). \tag{5.4}$$

Substituting Eq. 5.4 into Eq. 5.3, we obtain the $\rho(T)$ in the normal state

$$\rho(T) = \frac{m^*}{n_n e^2}\left(\frac{1}{\tau_{\rm i}} + \frac{T}{a}\right), \qquad (T > T_{\rm CDW}), \tag{5.5}$$

Then, by differentiating Eq. 5.5 with temperature, we obtain the temperature derivative of the resistivity ($\mathrm{d}\rho(T)/\mathrm{d}T$) in the normal state

$$\frac{\mathrm{d}\rho(T)}{\mathrm{d}T} = \frac{m^*}{n_n e^2 a}, \qquad (T > T_{\rm CDW}). \tag{5.6}$$

Next, we consider that a CDW gap opens on a part of the Fermi surface at $T_{\rm CDW}$ and the size of the gap changes below $T_{\rm CDW}$ obeying the temperature dependence of the gap function in the BCS theory. The $n(T)$ in this case is the sum of the electron density on the remaining Fermi surface and the density of thermally excited electrons beyond the CDW gap. Then, the $n(T)$ is expressed as

$$n(T) = n_n(1-p) + n_n p \exp\left(-\frac{2\Delta(T)}{k_{\rm B}T}\right), \qquad (T \leq T_{\rm CDW}), \tag{5.7}$$

where p ($0 < p < 1$) is the disappearance ratio of the Fermi surface due to the CDW transition, $\Delta(T)$ is the size of the CDW gap, and $k_{\rm B}$ is the Boltzmann constant. To simplify the calculation, we approximate $\Delta(T)$ guided by the BCS theory with the hyperbolik function expressed as

$$\begin{aligned}\Delta(T) &\approx \Delta(0)\tanh\left\{1.74\left(-1+\frac{T_{\rm CDW}}{T}\right)^{0.5}\right\} \\ &= 1.76 k_{\rm B} T_{\rm CDW}\tanh\left\{1.74\left(-1+\frac{T_{\rm CDW}}{T}\right)^{0.5}\right\},\end{aligned} \tag{5.8}$$

where $\Delta(0)$ is the size of the gap at 0 K, which is equal to $1.76 k_{\rm B} T_{\rm CDW}$. Figure 5.1 shows the temperature dependence of the $\Delta(T)$. Substituting Eq. 5.8 into Eq. 5.7 and substituting tha obtained equation into into Eq. 5.3, we obtain the $\rho(T)$ in the CDW

state

$$\rho(T) = \frac{m^*}{n_n e^2}\left(\frac{1}{\tau_{\rm i}} + \frac{T}{a}\right) \frac{1}{1 - p + p\exp\left[-\dfrac{3.52T_{\rm CDW}\tanh\left\{1.74\left(-1+\dfrac{T_{\rm CDW}}{T}\right)^{0.5}\right\}}{T}\right]}, \quad (T \leq T_{\rm CDW}). \tag{5.9}$$

Moreover, differentiating both sides of Eq. 5.5 with T, we obtain the $\mathrm{d}\rho(T)/\mathrm{d}T$ in the CDW state

$$\begin{aligned}\frac{\mathrm{d}\rho(T)}{\mathrm{d}T} = \frac{m^*}{n_n e^2 a}\Bigg\{ & \frac{1}{1 - p + p\exp\left[-\dfrac{3.52T_{\rm CDW}\tanh\left\{1.74\left(-1+\dfrac{T_{\rm CDW}}{T}\right)^{0.5}\right\}}{T}\right]} \\ & - \left(\frac{a}{\tau_{\rm i}} + T\right) p\exp\left[-\frac{3.52T_{\rm CDW}\tanh\left\{1.74\left(-1+\dfrac{T_{\rm CDW}}{T}\right)^{0.5}\right\}}{T}\right] \\ & \times \left[\frac{3.0624T_{\rm CDW}^2 \mathrm{sech}\left\{1.74\left(-1+\dfrac{T_{\rm CDW}}{T}\right)^{0.5}\right\}^2}{\left(-1+\dfrac{T_{\rm CDW}}{T}\right)^{0.5} T^3} + \frac{3.52T_{\rm CDW}\tanh\left\{1.74\left(-1+\dfrac{T_{\rm CDW}}{T}\right)^{0.5}\right\}}{T^2}\right] \\ & \div \left(1 - p + p\exp\left[-\frac{3.52T_{\rm CDW}\tanh\left\{1.74\left(-1+\dfrac{T_{\rm CDW}}{T}\right)^{0.5}\right\}}{T}\right]\right)^2\Bigg\}, \\ & (T \leq T_{\rm CDW}). \end{aligned} \tag{5.10}$$

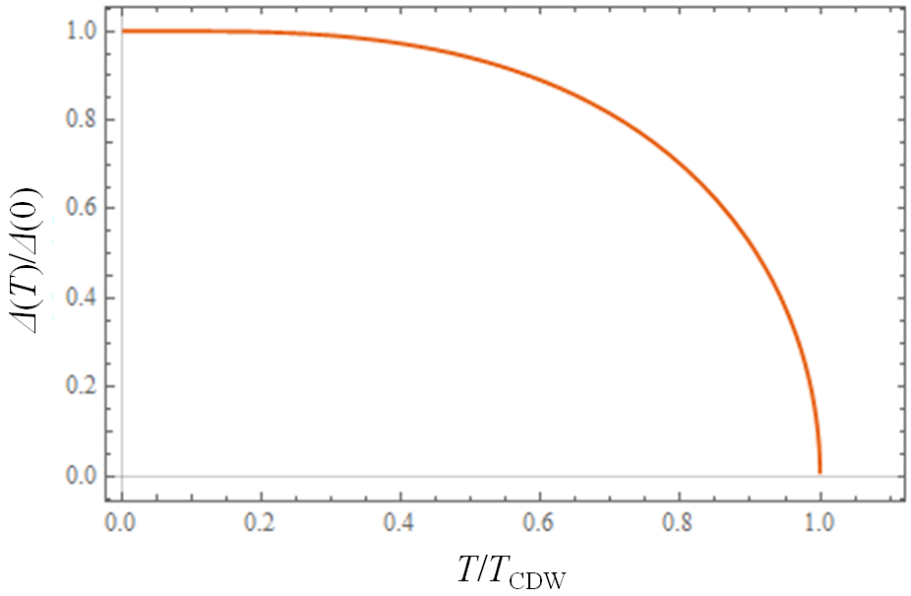

Figure 5.1: The CDW gap function expressed in Eq. 5.8.

As an example, we shows the temperature dependence of the $n(T)$, $\rho(T)$, and $\mathrm{d}\rho(T)/\mathrm{d}T$ in Fig. 5.2, Fig. 5.3, and Fig. 5.4, respectively, when $T_{\mathrm{CDW}} = 100$ K and $\tau_{\mathrm{i}}/\tau_{\mathrm{p}}(300\ \mathrm{K}) = 50$ (*i.e.*, $\tau_{\mathrm{i}}/a = 1/6$). The $n(T)$ suddenly decreases at the T_{CDW} and the decrease in the $n(T)$ becomes gentle as temperature goes down. The rate of decrease in the $n(T)$ below the T_{CDW} increases with increasing p. In the temperature dependence of $\rho(T)$, a hump is observed at the T_{CDW} and the size of the hump increases as p increases. In Fig 5.4, the $\mathrm{d}R/\mathrm{d}T$ for all values of p diverges to minus infinity at the T_{CDW} and increases with a downward curvature with decreasing temperature. That is, the temperature dependence of the $\mathrm{d}R/\mathrm{d}T$ commonly shows a "γ"-shaped dip.

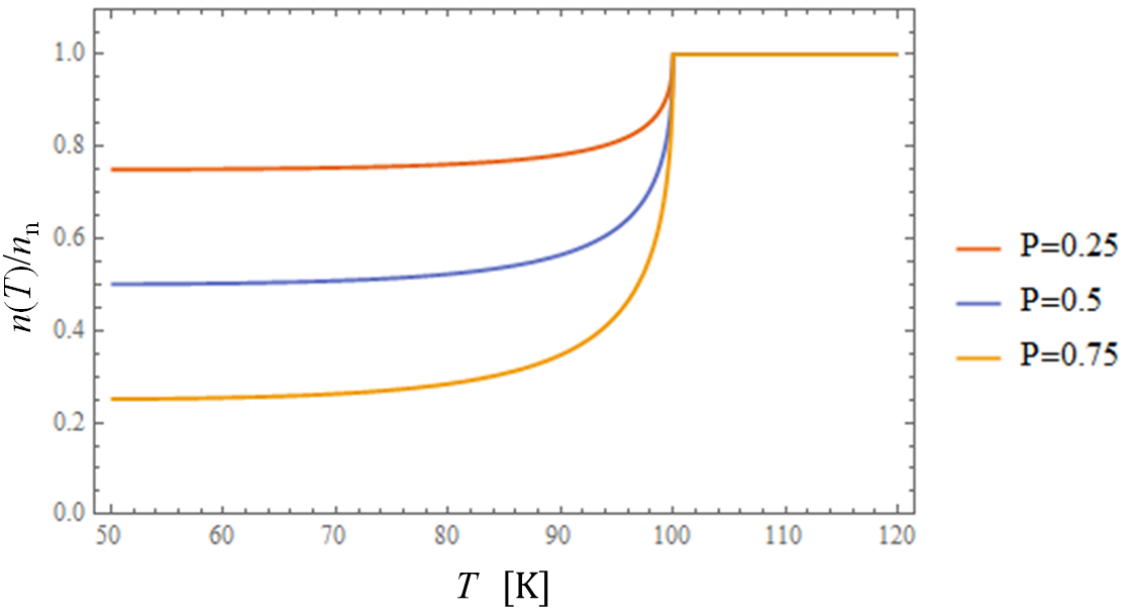

Figure 5.2: The temperature dependence of the density of conduction electrons expressed in Eq. 5.4 and Eq. 5.7 when $T_{\mathrm{CDW}} = 100$ K.

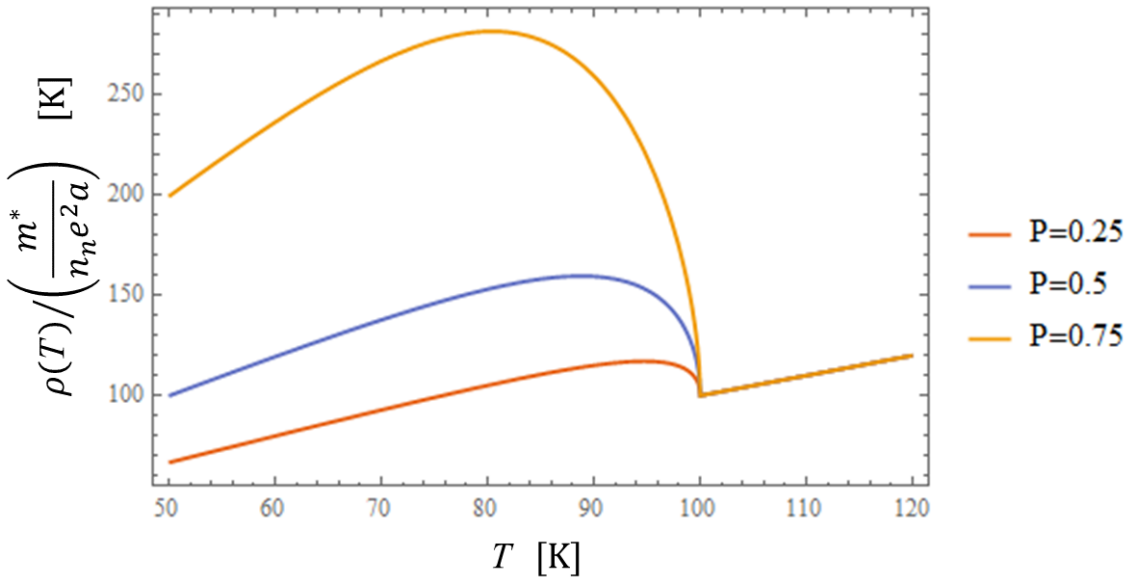

Figure 5.3: The temperature dependence of the resistivity expressed in Eq. 5.5 and Eq. 5.9 when $T_{\mathrm{CDW}} = 100$ K and $\tau_{\mathrm{i}}/\tau_{\mathrm{p}}(300\ \mathrm{K}) = 50$. The resistivity is normalized by the coefficient independent of temperature.

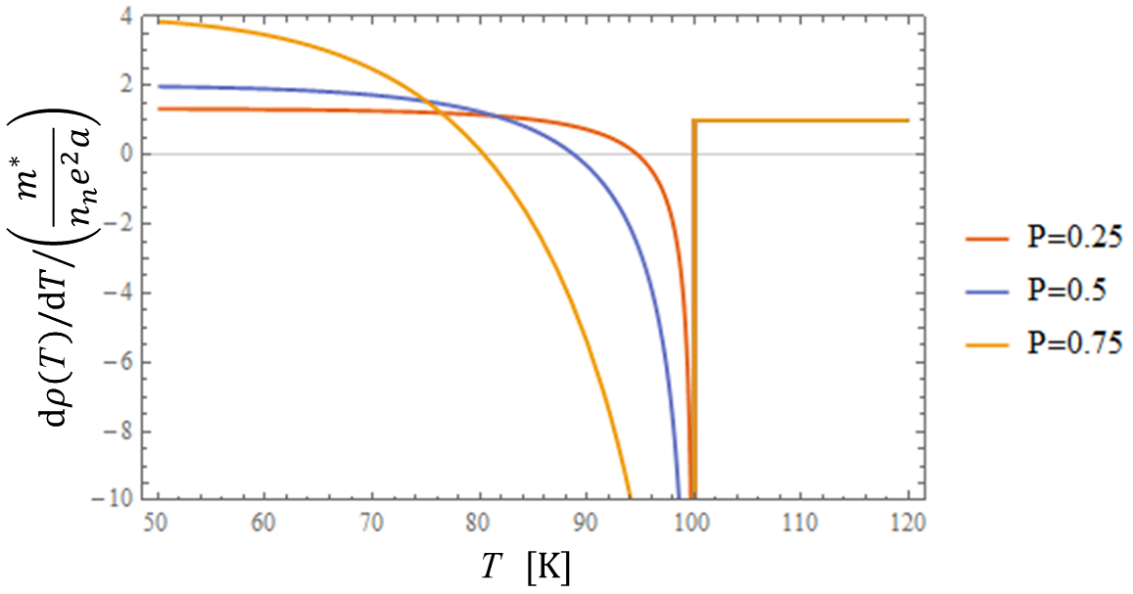

Figure 5.4: The temperature derivative of the resistivity expressed in Eq. 5.6 and Eq. 5.10 when $T_{\mathrm{CDW}} = 100$ K and $\tau_{\mathrm{i}}/\tau_{\mathrm{p}}(300\ \mathrm{K}) = 50$. The derivative is normalized by the coefficient independent of temperature.

Acknowledgements

I would like to express my appreciation to Prof. S. Tanda for accepting me who came from the Faculty of Fisheries and for making efforts so far for my doctorate degree. I have learned the importance of understanding things universally from him. I would like to express my sincere gratitude to Prof. K. Yamaya for supporting my Ph.D study continuously and teaching many important things. I could enjoy my study thanks to him. I hope that he will stay healthy and be active forever. I would like to thank Prof. S. Takayanagi, Prof. K. Ichimura, Prof. T. Matsuura, Prof. T. Kurosawa, Prof. H. Nobukane, Prof. T. Sakoda, Prof. S. Yasuzuka and Prof. P. Monceau for useful discussions, experimental supports, and their encouragement. I would like to acknowledge to Prof. S. Noro for performing the single crystal X-ray diffraction analysis. I am grateful to the members of the Topology Science and Technology Laboratory and Ms. S. Suzuki for their cooperation.

This study is supported by a grant-in-aid for science research from Hokkaido University Clark Memorial Foundation.

Finally, I would like to thank my parents for their understanding and encouragement so far.

References

[1] J. G. Bednorz and K.A. Müller, Z. Phys. B - Condensed Matter **64**, 189 (1986).

[2] L. Gao, Y. Y. Xue, F. Chen, Q. Xiong, R. L. Meng, D. Ramirez, C. W. Chu, J. H. Eggert, and H. K. Mao, Phys. Rev. B **50**, 4260(R) (1994).

[3] A. P. Drozdov, M. I. Eremets, I. A. Troyan, V. Ksenofontov, and S. I. Shylin, Nature Phys. **525**, 73 (2015).

[4] S. Yasuzuka, K. Murata, T. Fujimoto, M. Shimotori, and K. Yamaya, J. Phys. Soc. Jpn. **74**, 1782 (2005).

[5] E. Morosan, H. W. Zandbergen, B. S. Dennis, J. W. G. Bos, Y. Onose, T. Klimczuk, A. P. Ramirez, N. P. Ong, and R. J. Cava, Nat. Phys. **2**, 544 (2006).

[6] A. F. Kusmartseva, B. Sipos, H. Berger, L. Forró, and E. Tutiš, Phys. Rev. Lett. **103**, 236401 (2009).

[7] B. Sipos, A. F. Kusmartseva, A. Akrap, H. Berger, L. Forró, and E. Tutiš, Nature Mater. **7**, 960 (2008).

[8] L. J. Li, W. J. Lu, X. D. Zhu, L. S. Ling, Z. Qu, and Y. P. Sun, Europhys. Lett. **97**, 67005 (2012).

[9] X. Zhu, W. Ning, L. Li, L. Ling, R. Zhang, J. Zhang, K. Wang, Y. Liu, L. Pi, Y. Ma, H. Du, M. Tian, Y. Sun, C. Petrovic, and Y. Zhang, Sci. Rep. **6**, 26974 (2016).

[10] P. Monceau, Advances in Physics. **61**, 325 (2012).

[11] P. Monceau, Physica B. **460**, 2 (2015).

[12] T. Valla, A. V. Fedorov, P. D. Johnson, P-A. Glans, C. McGuinness, K. E. Smith, E. Y. Andrei, and H. Berger, Phys. Rev. Lett. **92**, 086401 (2004).

[13] K. Sugawara, Y. Nakata, R. Shimizu, P. Han, T. Hitosugi, T. Sato, and T. Takahashi, ACS Nano. **10**, 1341 (2016).

[14] R. Yomo, K. Yamaya, M. Abliz, M. Hedo and Y. Uwatoko, Phys. Rev. B **71**, 132508 (2005).

[15] K. Kawabata, J. Phys. Soc. Jpn. **54**, 762 (1985).

[16] A. M. Novello, M. Spera, A. Scarfato, A. Ubaldini, E. Giannini, D. R. Bowler, and Ch. Renner, Phys. Rev. Lett. **118**, 017002 (2017).

[17] A. Kogar, G. A. de la Pena, Sangjun Lee, Y. Fang, S. X. -L. Sun, D. B. Lioi, G. Karapetrov, K. D. Finkelstein, J. P. C. Ruff, P. Abbamonte, and S. Rosenkranz, Phys. Rev. Lett. **118**, 027002 (2017).

[18] E. Bjerkelund and A. Kjekshus, Acta Chem. Scand. **19**, 701 (1965).

[19] E. Bjerkelund, J. H. Fermor, and A. Kjekshus, Acta Chem. Scand. **20**, 1836 (1966).

[20] A. Meerschaut and J. Rouxel, J. Less Common Metals **39**, 197 (1975).

[21] J. Rijnsdorp and F. Jellinek, J. Solid State Chem. **25**, 325 (1978).

[22] M. Yamamoto, J. Phys. Soc. Jpn. **45**, 431 (1978).

[23] E. Canadell, I. E. -I. Rachidi, J. P. Pouget, P. Gressier, A. Meerschaut, J. Rouxel, D. Jung, M. Evain, and M. -H. Whangbo, Inorg. Chem. **29**, 1401 (1990).

[24] N. P. Ong and P. Monceau, Phys. Rev. B **16**, 3443 (1977).

[25] T. Sambongi, K. Tsutsumi, Y. Shiozaki, M. Yamamoto, K. Yamaya, and Y. Abe, Solid State Commun. **22**, 729 (1977).

[26] Z. Z. Wang, P. Monceau, H. Salva, C. Roucau, L. Guemas, and A. Meerschaut, Phys. Rev. B **40**, 11589 (1989).

[27] T. Sambongi, M. Yamamoto, K. Tsutsumi, Y. Shiozaki, K. Yamaya, and Y. Abe, J. Phys. Soc. Jpn. **42**, 1421 (1977).

[28] H. P. Geserich, G. Scheiber, F. Lévy, and P. Monceau, Physica B **143**, 174 (1986).

[29] T. Takoshima, M. Ido, K. Tsutsumi, T. Sambongi, S. Honma, K. Yamaya, and Y. Abe, Solid State Commun. **35**, 911 (1980).

[30] N. P. Ong and J. W. Brill, Phys. Rev. B **18**, 5265 (1978).

[31] A. Perucchi, C. Søndergaard, S. Mitrovic, M. Grioni, N. Barisic, H. Berger, L. Forró, and L. Degiorgi, Eur. Phys. J. B **39**, 433 (2004).

[32] M. N. Regueiro, Solid State Commun. **60**, 797 (1986).

[33] T. Sambongi, M. Yamamoto, K. Tsutsumi, Y. Shiozaki, K. Yamaya, and Y. Abe, J. Phys. Soc. Jpn. **42**, 1421 (1977).

[34] K. Yamaya and G. Oomi, J. Phys. Soc. Jpn. **51**, 3512 (1982).

[35] T. M. Tritt, E. P. Stillwell, and M. J. Skove, Phys. Rev. B **34**, 6799 (1986).

[36] T. Tsuneta, Ph. D. thesis, Hokkaido University, 2004.

[37] A. A. Sinchenko, P. Lejay, and P. Monceau, Phys. Rev. B **85**, 241104(R) (2012).

[38] J. Li, J. Peng, S. Zhang, and G. Chen, Phys. Rev. B **96**, 174510 (2017).

[39] S. Takahashi, T. Sambongi, J. W. Brill, and W. Roark, Solid State Commun. **49**, 1031 (1984).

[40] T. M. Rice and G. K. Scott, Phys. Rev. Lett. **35**, 120 (1975).

[41] M. Morita and K. Yamaya, Jpn. J. Appl. Phys. **26**, 975 (1987).

[42] S. Nagata, S. Ebisu, T. Aochi, Y. Kinoshita, S. Chikazawa, and K. Yamaya, J. Phys. Chem. Solids. **52**, 761 (1991).

[43] P. Haen, F. Lapierre, P. Monceau, M. Núñez Regueiro and J. Richard, Solid State Commun. **26**, 725 (1978).

[44] D. Bucheli, S. Caprara, C. Castellani and M. Grilli, New J. Phys. **15**, 023014 (2013).

[45] S. Caprara, J. Biscaras, N. Bergeal, D. Bucheli, S. Hurand, C. Feuillet-Palma, A. Rastogi, R. C. Budhani, J. Lesueur and M. Grilli, Phys. Rev. B **88**, 020504(R) (2013).

[46] G. E. D. K. Prawiroatmodjo, F. Trier, D. V. Christensen, Y. Chen, N. Pryds and T. S. Jespersen, Phys. Rev. B **93**, 184504 (2016).

[47] L. A. Turkevich and R. A. Klemm, Phys. Rev. B **19**, 2520 (1979).

[48] S. Kagoshima, H. Nagasawa, and T. Sambongi, *One-Dimensional Conductors* (Springer-Verlag, Berlin Heidelberg, 1988).

[49] J. M. Tranquada, B. J. Sternlieb, J. D. Axe, Y. Nakamura, and S. Uchida, Nature **375**, 561 (1995).